Acta Geotechnica (2017) 12:827–847
DOI 10.1007/s11440-016-0518-9

RESEARCH PAPER

A one-dimensional viscoelastic and viscoplastic constitutive approach to modeling the delayed behavior of clay and organic soils

Aldo Madaschi[1,2] · **Alessandro Gajo**[1]

Received: 28 April 2016 / Accepted: 14 December 2016 / Published online: 30 January 2017

Abstract Accurate modeling of the time-dependent behavior of geomaterials is of great importance in a number of engineering structures interacting with soft, highly compressible clay layers or with organic clays and peats. In this work, a uniaxial constitutive model, based on Perzyna's overstress theory and directly extendible to multiaxial stress conditions, is formulated and validated. The proposed constitutive approach essentially has three innovative aspects. The first concerns the implementation of two viscoplastic mechanisms within Perzyna's theory in order to distinguish between short-term (quasi-instantaneous) and long-term plastic responses. Similarly, elastic response is simulated by combining an instantaneous and a long-term viscous deformation mechanism. The second innovative aspect concerns the use of a bespoke logarithmic law for viscous effects, which has never been used before to simulate delayed soil behavior (as far as the authors are aware). The third concerns the model's extensive validation by simulating a number of different laboratory test results, including conventional and unconventional oedometer tests with small and large load increments/decrements and wide and narrow loading/unloading cycles, constant rates of stress and strain tests, and oedometer tests performed in a Rowe consolidation cell with measurement of pore pressure dissipation.

✉ Alessandro Gajo
alessandro.gajo@unitn.it

[1] Department of Civil, Environmental and Mechanical Engineering, University of Trento, Trento 38123, Italy

[2] Present Address: School of Architecture, Civil and Environmental Engineering, ENAC, Laboratory of Soil Mechanics, LMS, École Polytechnique Fédérale de Lausanne, EPFL, GC Station 18, 1015 Lausanne, Switzerland

Keywords Organic soils · Primary consolidation · Secondary compression · Softclays · Viscoelasticity · Viscoplasticity

1 Introduction

The need for reliable constitutive models of the time-dependent behavior of soils has been increasing in recent years due to the use of foundation soils composed of very soft, highly compressible clay layers (typically in coastal areas) or even of organic clays and peats (as often encountered in mountain areas). In most of such cases, the soils' behavior over time is generally too important an issue to be ignored [4]. One of the challenges for geotechnical engineers is to predict the long-term response of these soils when submitted to complicated loading histories, involving either wide loading/unloading cycles or small load increments/decrements, applied after a phase of creep or relaxation, or to sudden changes in strain rates.

Numerous constitutive models describing the time-dependent behavior of clays have been proposed in the literature. Most of them were reviewed in a fairly recent, thorough review by Liingaard et al. [24], so there is no need to repeat the process here, and the interested reader can refer to Liingaard et al. [24] for a complete literature review and to Madaschi and Gajo [28] for a review of the most recent works on multiaxial models. It is just worth recalling here that Liingaard et al. [24] suggested the following general classification:

- *empirical models* obtained by fitting experimental results, which are generally valid only for specific boundary and loading conditions;

- *rheological models* focusing on uniaxial conditions, and based on a differential representation (which can be visualized in the form of elastic springs, plastic sliders, or viscous dashpots), on engineering theories of creep, or on the hereditary approach;
- *general stress–strain–time models*, which provide a multiaxial formulation, usually expressed in incremental form (and suitable for implementing in finite element codes, e.g., [39, 41]).

This classification is still valid and can be applied to the most recent works (e.g., [16, 21]), although it should be integrated with a new class of constitutive models based on methods for upscaling from micro- to macroaspects, using the framework of dual porosity/dual permeability for instance [5, 7, 49] or considering the effects of local dehydration processes [40]. Such micromechanically derived approaches have not been developed to a level suitable for describing the full complexity of delayed soil response induced by complex loading histories, however, and that is why conventional viscoplastic models are still the object of ongoing research [30, 45].

The constitutive model proposed in this work belongs to the second and third categories. It can be classified as a uniaxial model based on a differential representation in which nonlinear springs, sliders, and viscous dashpots are used. The nonlinearity of these elementary mechanical elements was deduced from empirical models, and particularly from the strain rate approach (the so-called isotache model) first proposed by Suklje [47], and later investigated in detail by Leroueil et al. [23]. The proposed uniaxial model is directly extendible to multiaxial stress conditions, however, as shown in two companion papers [27, 28] describing the proposed model implemented for multiaxial stress conditions within the framework of Perzyna's overstress theory.

A peculiar characteristic of the proposed model concerns the distinction between short-term (instantaneous or quasi-instantaneous) vis-à-vis long-term elastic and plastic responses. This concept was first proposed by Bjerrum [4], and later by Di Benedetto et al. [8], as a helpful framework for understanding the rheology of soil behavior. To the best of the authors' knowledge, however, the rigorous implementation of this concept in a constitutive model was only proposed by Borja and Kavazanjian [6], using the concept of *reference* volumetric and deviatoric *times*, and by Kaliakin and Dafalias [17], within a bounding surface approach. Both of said approaches neglected viscoelasticity and assumed the existence of an instantaneous and a viscous plastic mechanism (i.e., a [IV] viscoplastic model). More recently, Madaschi and Gajo [27] proposed a different [IV] viscoplastic approach consisting of two yield surfaces: the external yield surface is a conventional elastoplastic yield surface describing the instantaneous plastic mechanism, while the inner yield surface is a Perzyna-type, viscous yield surface describing the viscoplastic, long-term, deformation mechanism. The consistency condition is strictly imposed on both yield surfaces. In contrast, Madaschi and Gajo [28] investigated the role of two viscoplastic mechanisms with different viscosities (i.e., a [VV] viscoplastic model), such that both the inner and the outer yield surfaces follow two different viscoplastic mechanisms according to Perzyna's theory. Although the [IV] formulation [27] leads to a simplification of the numerical analysis and is suitable for analyzing many applicative problems [25], it cannot be used to simulate the delayed behavior observed in undrained triaxial tests [28].

For uniaxial problems, the response of a [IV] viscoplastic model was recently explored by Madaschi and Gajo [25], but a detailed analysis of [VV] models is still lacking. The model proposed in this paper is the uniaxial version of the multiaxial model proposed by Madaschi and Gajo [28], and it is based on a conventional approach to Perzyna's viscoplasticity, with a [VV] viscoplastic response. No *reference time* is included in the hardening relationships, thus avoiding the difficulties that usually arise when it comes to defining an equivalent time in the case of complicated loading histories. In addition, the proposed model is based on a strain decomposition that differs from the one proposed by Borja and Kavazanjian [6] and Kaliakin and Dafalias [17], in order to enable a consistent model formulation within Perzyna's viscoplasticity.

The proposed constitutive approach essentially has the following innovative aspects. The first is the above-mentioned implementation for uniaxial problems of a constitutive model with two viscoplastic mechanisms (i.e., a [VV] viscoplastic model) within a conventional Perzyna's theory. Viscoelasticity is also taken into account, and elastic deformations are assumed to be given by the sum of an instantaneous short-term mechanism and a long-term, viscous deformation mechanism (i.e., a [IV] viscoelasticity).

The second novel aspect of the proposed model concerns the use of a specially adapted logarithmic law for the viscous effects, which has never been used before to simulate delayed soil behavior (as far as the authors are aware). This expression is used to simulate both elastic and plastic viscous strains, making the proposed model one of the few capable of modeling both the viscoelasticity and the viscoplasticity of soils. The resulting behavior depends on both strain amplitude and strain rate, ϵ and $\dot{\epsilon}$. The proposed logarithmic relationship consistently simulates all the well-accepted empirical laws concerning the delayed behavior of soils and proves particularly suitable for enhancing the rate of numerical convergence.

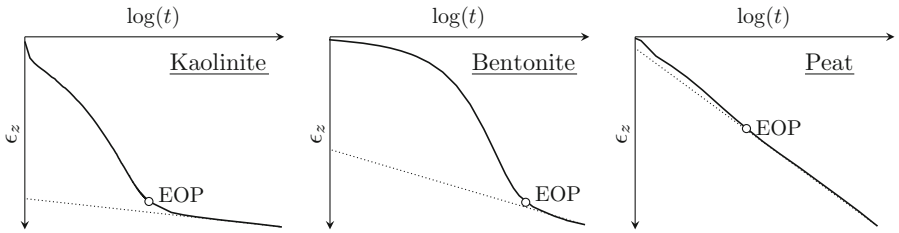

Fig. 1 Time-dependent behavior of different types of soil in oedometric condition at constant stress [25]

The third novel aspect of this work is the model's extensive and exhaustive validation. The model's simulations are validated below by means of a detailed comparison with the experimental results recently presented by Madaschi and Gajo [26], concerning two different peats submitted to a number of conventional and unconventional oedometer tests that involved multistage loading (MSL) with small and large load increments/decrements, and wide and narrow loading/unloading cycles, conducting tests at constant rate of stress (CRSS) and strain (CRS), and measuring pore pressure dissipation in a Rowe consolidation cell (RC-MSL). In most of these tests, both reversible and irreversible deformations have been explored. Experimental results obtained on inorganic clays are considered too.

The proposed model results particularly appropriate for distinguishing the behavior of inorganic clays from that of organic clays and peats. In particular, short-term deformations in inorganic clays are larger than long-term deformations, whereas the short-term behavior of organic soils is negligible. The model reliably simulates all the oedometer tests, capturing the following aspects: the isotache concept [47], which postulates the existence of a unique stress–strain curve for each strain rate; the preconsolidation pressure induced by aging at a constant stress [4]; the effects of the strain rate on the preconsolidation pressure [23]; the concept of constant C_α/C_c ratio [32, 33, 48]; and the secondary deformations induced by a small stress increment ratio [10, 37, 38].

The present paper is organized as follows: the constitutive model and its numerical implementation are presented in Sect. 2; the model's typical outputs are illustrated in Sect. 3; the parametric analysis is described in Sect. 4; some suggestions for calibrating the model are provided in Sect. 5; comparisons are drawn between the model's simulations and experimental results in Sect. 6, and Sect. 7 contains some concluding comments.

2 Formulation of the constitutive model

The proposed constitutive model was deduced from measurements of the time-dependent, 1D response of different types of organic and inorganic soils available in the literature [23, 26]. Although the delayed response of fine-grained soils under oedometric conditions is strongly related to their mineralogical composition, some aspects of soil response are common to all soils. These aspects can be summarized as follows:

- the evolution of the deformation in a creep test (i.e., under constant stress) is generally linear on a logarithm of time plot, with a slope that is described by the coefficient of secondary compression C_α [4, 47];
- time-dependent deformations affect both the elastic and the plastic regime, so a soil's general behavior can be classified as both viscoelastic and viscoplastic;
- assuming in a first approximation that viscous deformations are linear on the logarithm of time plot throughout the primary consolidation stage (see the dotted line in Fig. 1), the relative amount of viscous deformation at the end of the primary consolidation stage with respect to the total deformation depends strongly on the nature of the soil considered: it may be very small in kaolinite, considerably larger in bentonite, and predominant in peats (Fig. 1).

The present constitutive model is developed referring to the effective stress, and the modeled time-dependent phenomena relate only to the viscosity of the solid skeleton. The coupling between the solid and liquid phases must be accounted for separately, by means of a hydromechanically coupled, 1D analysis. Stresses and strains are assumed to be positive in compression, based on the usual assumption in soil mechanics. For the sake of simplicity, the effective stresses are denoted with the symbol σ without the usual prime.

Starting from the above basic observations, we propose to model the soil's oedometric response with the rheological model shown in Fig. 2. The most important assumption for the model is that both elastic and plastic deformations comprise short-term and long-term fractions. Since soil deformation at the end of the primary consolidation stage is mainly attributable to the short-term mechanism (with a much smaller fraction due to the long-term mechanism), the short-term fraction of the deformation in the examples of Fig. 1 can be expected to be large for kaolinite and bentonite and negligible for peats.

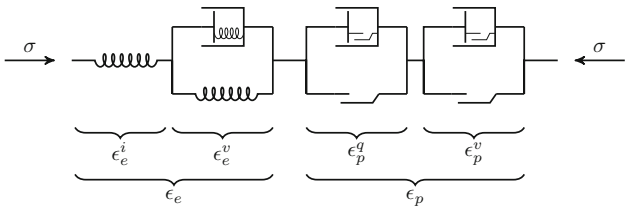

Fig. 2 Proposed rheological model

The simplest assumption for the short-term deformation mechanism is that this fraction is perfectly instantaneous. This has been assumed for the short-term elastic response, so wave propagation still has a finite velocity. The assumption of perfectly instantaneous, plastic behavior generates some inconsistencies, however, when the model is extended to multiaxial conditions (to simulate undrained triaxial tests on NC clays, for instance [28]), so the short-term plastic mechanism is assumed here to have a viscous nature. In fact, the simulation of undrained tests turns out to be affected mainly by the yield mechanism with the shortest response. As a result, if the short-term mechanism is assumed to be perfectly instantaneous, then there are no rate effects in the simulation of undrained triaxial tests (it is worth emphasizing that the inconsistency in the simulation of undrained tests does not appear if a single viscous yield mechanism is considered, as in [50]). The reliability of the assumption concerning the short-term response (whether perfectly instantaneous or quasi-instantaneous) is tested below by analyzing the pore pressure dissipation during primary consolidation.

The resulting rheological model consists of four elements (Fig. 2): the first two represent the elastic part, the last two the plastic (irreversible) part of the deformation. Both parts comprise a short-term and a long-term mechanism, so the decomposition of the total deformation is expressed by the following equation

$$\epsilon = \underbrace{\epsilon_{\mathrm{e}}^{i} + \epsilon_{\mathrm{e}}^{v}}_{\epsilon_{\mathrm{e}}} + \underbrace{\epsilon_{\mathrm{p}}^{q} + \epsilon_{\mathrm{p}}^{v}}_{\epsilon_{\mathrm{p}}}, \tag{1}$$

where 'e' and 'p' denote the type of deformation component (elastic and plastic, respectively), and the apex identifies the time-dependent nature of the deformation component ('i' for instantaneous, 'q' for quasi-instantaneous, 'v' for viscous). The proposed rheological approach has the advantage of preserving the intuitive breakdown of the total deformation into elastic and plastic parts (facilitating the model's calibration). On the other hand, the proposed breakdown of the strain complicates the numerical implementation of the model by comparison with rheological models based on breaking down the stress (e.g., the generalized Maxwell model [14]) because each fraction of the total strain increment has to be assessed by solving a highly nonlinear system of equations.

Perzyna [43] and, later on, Adachi and Oka [2] both proposed the static equilibrium state concept, defined as the state at which plastic strain rates become zero. This concept was recently used by Qiao et al. [45] too, who denoted it as *final stable state*. In the model proposed here, the *final stable state* (when viscous effects are negligible) is assumed to follow the usual, inviscid stress–strain response of clays under one-dimensional conditions, when the compression response in terms of vertical strain versus the logarithm of stress is presumably bilinear, with an initial slope κ for the purely elastic response and λ for elasto-plastic strains.

The proposed model extends to viscous materials the accepted concepts concerning the inviscid stress–strain response of clays under one-dimensional conditions by splitting the elastic and plastic mechanisms into short- and long-term components, thus generating the following instantaneous and viscous elastic relationships.

$$\sigma_{\mathrm{e}}^{i} = \sigma_0 \ \exp\left(\frac{\epsilon_{\mathrm{e}}^{i} - \alpha_{\mathrm{e}}\,\epsilon_{\mathrm{e0}}}{\alpha_{\mathrm{e}}\,\kappa}\right) \tag{2a}$$

$$\sigma_{\mathrm{e}}^{v} = \sigma_0 \ \exp\left(\frac{\epsilon_{\mathrm{e}}^{v} - (1-\alpha_{\mathrm{e}})\,\epsilon_{\mathrm{e0}}}{(1-\alpha_{\mathrm{e}})\,\kappa}\right)\left[1 + \psi_{\mathrm{e}}(\dot{\epsilon}_{\mathrm{e}}^{v})\right], \tag{2b}$$

where σ_0 is the reference pressure (usually 1 kPa), corresponding to the initial elastic strain ϵ_{e0} (usually assumed to be null), $\psi_{\mathrm{e}}(\dot{\epsilon}_{\mathrm{e}}^{v})$ is a viscosity function defined in Sect. 2.1, and α_{e} is a partition coefficient, ranging between 0 and 1. The effect of the partition coefficient is to split the elastic deformation into an instantaneous and a delayed part, so that a purely viscous response is obtained when $\alpha_{\mathrm{e}} \to 0$, and a purely instantaneous response is simulated when $\alpha_{\mathrm{e}} \to 1$. Note that, in order to guarantee equilibrium with the effective applied stress σ, the following equality must hold true $\sigma = \sigma_{\mathrm{e}}^{i} = \sigma_{\mathrm{e}}^{v}$. When the *final stable state* is reached [namely $\dot{\epsilon}_{\mathrm{e}}^{v} = 0$, and therefore $\psi_{\mathrm{e}}(\dot{\epsilon}_{\mathrm{e}}^{v}) = 0$], then $\epsilon_{\mathrm{e}}^{i} = \alpha_{\mathrm{e}}\,\epsilon_{\mathrm{e}}$ and $\epsilon_{\mathrm{e}}^{v} = (1-\alpha_{\mathrm{e}})\,\epsilon_{\mathrm{e}}$, thus recovering the usual Cam–Clay elastic relationship

$$\sigma = \sigma_{\mathrm{e}}^{i} = \sigma_{\mathrm{e}}^{v} = \sigma_0 \ \exp\left(\frac{\epsilon_{\mathrm{e}} - \epsilon_{\mathrm{e0}}}{\kappa}\right) \tag{3}$$

The same approach is used for the quasi-instantaneous, scarcely viscous and for the long-term, highly viscous parts of the plastic strain, and thus,

$$\sigma_{\mathrm{p}}^{q} = \sigma_{\mathrm{pc}}^{q}\left[1 + \psi_{\mathrm{p}}^{q}(\dot{\epsilon}_{\mathrm{p}}^{q})\right] \tag{4a}$$

$$\sigma_{\mathrm{p}}^{v} = \sigma_{\mathrm{pc}}^{v}\left[1 + \psi_{\mathrm{p}}^{v}(\dot{\epsilon}_{\mathrm{p}}^{v})\right], \tag{4b}$$

where $\psi_{\mathrm{p}}^{q}(\dot{\epsilon}_{\mathrm{p}}^{q})$ and $\psi_{\mathrm{p}}^{v}(\dot{\epsilon}_{\mathrm{p}}^{v})$ have the same meaning as $\psi_{\mathrm{e}}(\dot{\epsilon}_{\mathrm{e}}^{v})$, and the two stresses on the sliders, σ_{pc}^{q} and σ_{pc}^{v}, act as static yield stresses

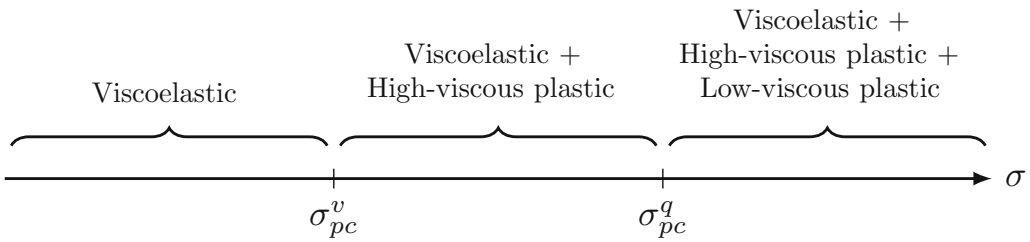

Fig. 3 Scheme of the response of the model

$$\sigma^q_{\mathrm{pc}} = \sigma_0 \ \exp\left(\frac{\epsilon^q_{\mathrm{p}} - \alpha_{\mathrm{p}}\,\epsilon_{\mathrm{p0}}}{\alpha_{\mathrm{p}}\,(\lambda-\kappa)}\right) \tag{5a}$$

$$\sigma^v_{\mathrm{pc}} = \sigma_0 \ \exp\left(\frac{\epsilon^v_{\mathrm{p}} - (1-\alpha_{\mathrm{p}})\,\epsilon_{\mathrm{p0}}}{(1-\alpha_{\mathrm{p}})(\lambda-\kappa)}\right), \tag{5b}$$

where ϵ_{p0} is the initial plastic strain (usually assumed to be null) occurring at $\sigma = \sigma_0$. Note that α_{p} has the same role as α_{e} in separating the plastic strains into a short- and a long-term fraction. To ensure equilibrium (i.e., the consistency) between the various rheological components under the applied stress σ, the following equality must hold: $\sigma = \sigma^i_{\mathrm{e}} = \sigma^v_{\mathrm{e}} = \sigma^q_{\mathrm{p}} = \sigma^v_{\mathrm{p}}$. Equivalently to the viscoelastic mechanism, when the *final stable state* is reached (namely $\dot{\epsilon}^q_{\mathrm{p}} = \dot{\epsilon}^v_{\mathrm{p}} = 0$, and therefore $\psi^q_{\mathrm{p}}(\dot{\epsilon}^q_{\mathrm{p}}) = \psi^v_{\mathrm{p}}(\dot{\epsilon}^v_{\mathrm{p}}) = 0$) then $\epsilon^q_{\mathrm{p}} = \alpha_{\mathrm{p}}\,\epsilon_{\mathrm{p}}$ and $\epsilon^v_{\mathrm{p}} = (1-\alpha_{\mathrm{p}})\,\epsilon_{\mathrm{p}}$, thus recovering the usual Cam–Clay plastic relationship

$$\sigma = \sigma^q_{\mathrm{p}} = \sigma^v_{\mathrm{p}} = \sigma_0 \ \exp\left(\frac{\epsilon_{\mathrm{p}} - \epsilon_{\mathrm{p0}}}{\lambda-\kappa}\right). \tag{6}$$

Equation (5) represents two nonlinear hardening sliders, taking the plastic deformation into account. If the stress applied is less than the stress associated with the slider elements (acting as preconsolidation stresses), only the elastic spring mechanisms are active. If one or both preconsolidation stresses are exceeded, then the two elastic mechanisms plus one or both plastic mechanisms are active.

According to Perzyna' theory, the static yield stresses σ^q_{pc} and σ^v_{pc} depend on their respective plastic strains (namely $\sigma^q_{\mathrm{pc}} = \hat{\sigma}^q_{\mathrm{pc}}(\epsilon^q_{\mathrm{p}})$ and $\sigma^v_{\mathrm{pc}} = \hat{\sigma}^v_{\mathrm{pc}}(\epsilon^v_{\mathrm{p}})$), thus obeying a classical strain hardening rule. However, σ^q_{p} and σ^v_{p} can be considered as dynamic yield stresses, depending on both plastic strain and strain rate (namely $\sigma^q_{\mathrm{p}} = \tilde{\sigma}^q_{\mathrm{p}}(\epsilon^q_{\mathrm{p}}, \dot{\epsilon}^q_{\mathrm{p}})$ and $\sigma^v_{\mathrm{p}} = \tilde{\sigma}^v_{\mathrm{p}}(\epsilon^v_{\mathrm{p}}, \dot{\epsilon}^v_{\mathrm{p}})$), thus leading to a strain and strain rate hardening model. This is consistent with Perzyna's theory, according to which the static yield stresses are believed to have a more fundamental role as internal variables than the dynamic yield stresses.

The resulting response of the elastic and plastic dashpots is fairly innovative because it includes a dependence on both the strain amplitude and the strain rate, ϵ and $\dot{\epsilon}$. That is why the dashpots are denoted with a special symbol in Fig. 2.

It is worth emphasizing that, due to the short- and long-term nature of the two plastic mechanisms, σ^v_{pc} is always smaller than σ^q_{pc} (see Fig. 3), and the two yield stresses coincide with one another and with the applied stress σ (i.e., $\sigma = \sigma^q_{\mathrm{pc}} = \sigma^v_{\mathrm{pc}}$) only for very long times, at the *final stable state*, when the effects of the strain rates vanish.

Long-term (highly viscous) plastic deformations thus occur when σ lies between σ^v_{pc} and σ^q_{pc}, whereas both quasi-instantaneous (scarcely viscous) and long-term (highly viscous) plastic strains occur when σ is greater than σ^q_{pc} (see Fig. 3).

The viscosity functions $\psi_{\mathrm{e}}(\dot{\epsilon}^v_{\mathrm{e}})$, $\psi^q_{\mathrm{p}}(\dot{\epsilon}^q_{\mathrm{p}})$ and $\psi^v_{\mathrm{p}}(\dot{\epsilon}^v_{\mathrm{p}})$ govern the evolution of the viscous strains in relation to time and the state of stress, and they are expressed in terms of strain rates ($\dot{\epsilon}^v_{\mathrm{e}}$ for the viscoelastic mechanism, $\dot{\epsilon}^q_{\mathrm{p}}$ and $\dot{\epsilon}^v_{\mathrm{p}}$ for the viscoplastic one). The viscosity functions must vanish when the strain rate is null ($\dot{\epsilon}^v_{\mathrm{e}} = 0$, $\dot{\epsilon}^q_{\mathrm{p}} = 0$, and $\dot{\epsilon}^v_{\mathrm{p}} = 0$) to ensure the consistency of the model's output for extremely slow processes.

2.1 Choice of viscosity functions

The choice of the viscosity functions is crucial to the proper prediction of the delayed soil response and must be based on experimental observations of the material's behavior. In fine-grained soils, the typical strain–time response obtained by incremental loading oedometer tests with a large load increment is almost linear with the logarithm of time, after primary consolidation has come to an end (Fig. 1). This evidence is generally accepted and has been observed by many authors and in different soils [3, 4, 31, 35, 47].

Although the assumption of a linear log-time response certainly has strong limitations (see [50]) and cannot be applied up to infinitely long times, in the present work, the linearity of the log-time response was considered one of the most important aspects to simulate accurately in order to obtain consistent simulations of the experimental observations (on the laboratory time scale at least) and of the

isotache concept, so the plastic viscosity function was assumed to comprise a logarithmic branch smoothly linked to a polynomial expression close to the origin of the axis, namely,

$$\psi_{\mathrm{p}}^{k}(\dot{\epsilon}_{\mathrm{p}}^{k}) = \Gamma_{\mathrm{p}}^{k}\mathcal{A}, \tag{7}$$

where

$$\mathcal{A} = \begin{cases} \ln\left(\dfrac{\dot{\epsilon}_{\mathrm{p}}^{k}}{\dot{\epsilon}_{\mathrm{ref}}}\right) & \text{for } \dot{\epsilon}_{\mathrm{p}}^{k} > \beta\dot{\epsilon}_{\mathrm{ref}} \\ a\dot{\epsilon}_{\mathrm{p}}^{k} + b\left(\dot{\epsilon}_{\mathrm{p}}^{k}\right)^{2} + c\left(\dot{\epsilon}_{\mathrm{p}}^{k}\right)^{3} & \text{for } \dot{\epsilon}_{\mathrm{p}}^{k} \le \beta\dot{\epsilon}_{\mathrm{ref}} \end{cases}$$

and where the superscript k stands for $k = q$ (for the quasi-instantaneous, short-term mechanism) and $k = v$ (for the viscous, long-term mechanism), Γ_{p}^{q}, Γ_{p}^{v}, β, and $\dot{\epsilon}_{\mathrm{ref}}$ are four constitutive parameters, and the polynomial coefficients a, b, and c depend on a further constitutive parameter, γ, which defines the tangent of the viscosity function at the origin of the axis (see "Appendix"). It is worth adding that it will be shown below that the logarithmic function accurately simulates the soil's delayed behavior induced by complex loading histories.

It is worth noting that the viscosity function in Eq. (7) is derived from a proposal originally advanced by Malvern [29] and later adopted by Perzyna [42], namely

$$\psi_{\mathrm{p}}^{k}(\dot{\epsilon}^{k}) = \Gamma_{\mathrm{p}}^{k}\ln\left(\frac{\dot{\epsilon}^{k}}{\dot{\epsilon}_{\mathrm{ref}}} + 1\right) \tag{8}$$

which is numerically less convenient than Eq. (7), especially in the case of very low strain rates. In fact, Eq. (8) involves a much steeper tangent at the origin of the axes (Fig. 4). As a result, although Eqs. (7) and (8) may both lead to nonconvergence of the Newton–Raphson algorithm (thus requiring a line-search algorithm), Eq. (8) implies a much slower convergence rate.

The viscosity function proposed in Eq. (7) (and in Eq. 8 as well) is null for $\dot{\epsilon}^{v} = 0$ and is shown below to provide an almost linear response in a $\epsilon^{v} - \log t$ plot. The parameter $\dot{\epsilon}_{\mathrm{ref}}$ must be sufficiently smaller than the strain rates considered in a given application. As shown below, for high values of Γ_{p}, the creep curves tend to acquire a slightly downward concavity that could be made vanishingly small by assuming that the viscosity function consists of a second-order polynomial in the logarithmic strain rate. This possibility has not been fully investigated, however.

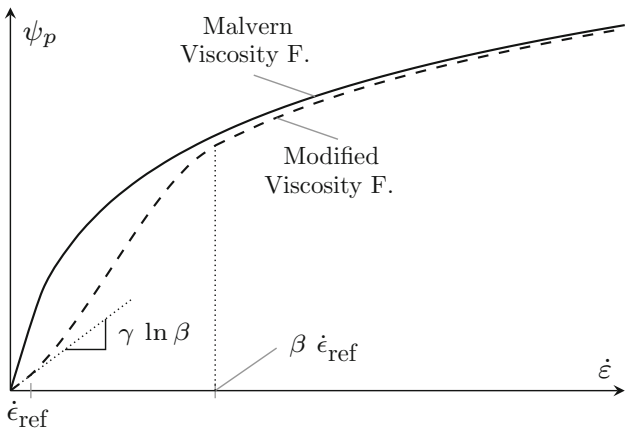

Fig. 4 Viscosity function

Figure 4 shows the comparison between the original Malvern viscosity function (Eq. 8) and the one proposed here (Eq. 7). At high strain rates, the two functions practically coincide, whereas slight differences appear for strain rates nearing $\dot{\epsilon}_{\mathrm{ref}}$.

Although the modified viscosity function (Eq. 7) is numerically more convenient than the original, the two formulations generate very similar strain–time responses, except for vanishingly small strain rates.

It is worth adding that in an approach envisaging a single viscous mechanism, Adachi and Oka [2] and Fodil et al. [9] used apparently similar logarithmic relationships, but they were actually very different from ours, and this prevented the proper simulation of the linearity on a log-time plot [9]. Many investigators (e.g., [16, 21]) used a viscosity function based on a power function of the plastic strain rate, which is less appropriate for reproducing the linearity of the creep strain response on a log-time plot [9].

The viscoelastic deformation is described by a similar viscosity function, namely,

$$\psi^{\mathrm{e}}(\dot{\epsilon}_{\mathrm{e}}^{v}) = \Gamma_{\mathrm{e}}\mathcal{B}, \tag{9}$$

where

$$\mathcal{B} = \begin{cases} \mathrm{sign}(\dot{\epsilon}_{\mathrm{e}}^{v})\ln\left(\dfrac{|\dot{\epsilon}_{\mathrm{e}}^{v}|}{\dot{\epsilon}_{\mathrm{ref}}}\right) & \text{for } |\dot{\epsilon}_{\mathrm{e}}^{v}| > \beta\dot{\epsilon}_{\mathrm{ref}} \\ a\dot{\epsilon}_{\mathrm{e}}^{v} + b\,\mathrm{sign}(\dot{\epsilon}_{\mathrm{e}}^{v})\left(\dot{\epsilon}_{\mathrm{e}}^{v}\right)^{2} + c\left(\dot{\epsilon}_{\mathrm{e}}^{v}\right)^{3} & \text{for } |\dot{\epsilon}_{\mathrm{e}}^{v}| \le \beta\dot{\epsilon}_{\mathrm{ref}} \end{cases}$$

and where Γ_{e} is a constitutive parameter. It is worth noting that the *sign* function is used here due to the possible existence of positive and negative $\dot{\epsilon}_{\mathrm{e}}^{v}$. Moreover, β, $\dot{\epsilon}_{\mathrm{ref}}$, and the coefficient γ (and thus a, b, and c) are equal to those employed for the viscoplastic strains (Eq. 7), so the viscoelastic and viscoplastic strains are described by similar viscosity functions that only differ quantitatively from one another, through the constitutive parameters Γ_{p}^{q}, Γ_{p}^{v}, and Γ_{e}.

2.2 Numerical integration of constitutive functions

The numerical implementation of the constitutive model described in the previous sections was done with a fully implicit back-Euler algorithm. Thus, once a strain increment $\Delta\epsilon$ is assigned (from the FEM code) in a given time step increment Δt, the strain increment is initially assumed

to be entirely elastic, whereas the discretized strain rate becomes equal to $\Delta\epsilon/\Delta t$. As a result, a nonlinear system of two equations must be solved first in order to assess the two elastic increments $\Delta\epsilon_{\mathrm{e}}^{i}$ and $\Delta\epsilon_{\mathrm{e}}^{v}$, from Eq. (2)

$$\exp\left(\frac{(\epsilon_{\mathrm{e}}^{i})_n+\Delta\epsilon_{\mathrm{e}}^{i}-\epsilon_{\mathrm{e}0}}{\alpha_{\mathrm{e}}\kappa}\right) = \exp\left(\frac{(\epsilon_{\mathrm{e}}^{v})_n+\Delta\epsilon_{\mathrm{e}}^{v}-\epsilon_{\mathrm{e}0}}{(1-\alpha_{\mathrm{e}})\kappa}\right)\left[1+\psi_{\mathrm{e}}\left(\frac{\Delta\epsilon_{\mathrm{e}}^{v}}{\Delta t}\right)\right] \tag{10a}$$

$$\Delta\epsilon=\Delta\epsilon_{\mathrm{e}}^{i}+\Delta\epsilon_{\mathrm{e}}^{v}, \tag{10b}$$

where $(\epsilon_{\mathrm{e}}^{i})_n$ and $(\epsilon_{\mathrm{e}}^{v})_n$ denote the instantaneous and viscoelastic strains assessed at the previous time step. The *elastic* stress computed by solving the nonlinear Eq. (10) constitutes the so-called *elastic predictor*. If the *elastic predictor* is smaller than both σ_{pc}^{v} and σ_{pc}^{q}, then the computed *elastic* stress is valid, and the next time step can be considered.

Alternatively, if the *elastic* stress is greater than the long-term viscous preconsolidation pressure σ_{pc}^{v}, then the long-term, highly viscous plastic mechanism is activated and the nonlinear system of three equations comprising Eq. (10a) and the following two additional equations (deduced from Eqs. (2b), (4a) and from the strain breakdown rule) needs to be solved

$$\exp\left(\frac{(\epsilon_{\mathrm{e}}^{i})_n+\Delta\epsilon_{\mathrm{e}}^{i}-\alpha_{\mathrm{e}}\,\epsilon_{\mathrm{e}0}}{\alpha_{\mathrm{e}}\,\kappa}\right) = \exp\left(\frac{(\epsilon_{\mathrm{p}}^{v})_n+\Delta\epsilon_{\mathrm{p}}^{v}-(1-\alpha_{\mathrm{p}})\,\epsilon_{\mathrm{p}0}}{(1-\alpha_{\mathrm{p}})(\lambda-\kappa)}\right)\left[1+\psi_{\mathrm{p}}^{v}\left(\frac{\Delta\epsilon_{\mathrm{p}}^{v}}{\Delta t}\right)\right], \tag{11a}$$

$$\Delta\epsilon=\Delta\epsilon_{\mathrm{e}}^{i}+\Delta\epsilon_{\mathrm{e}}^{v}+\Delta\epsilon_{\mathrm{p}}^{v}, \tag{11b}$$

where $(\epsilon_{\mathrm{p}}^{v})_n$ is the viscoplastic strain assessed at the previous time step, and there are three unknowns, namely $\Delta\epsilon_{\mathrm{e}}^{i}$, $\Delta\epsilon_{\mathrm{e}}^{v}$, and $\Delta\epsilon_{\mathrm{p}}^{v}$. If the computed stress $\sigma_{\mathrm{pc}}^{v}=\sigma_{\mathrm{e}}^{i}=\sigma_{\mathrm{e}}^{v}$ is smaller than σ_{pc}^{q}, then the computed stress is valid, and the next time step can be considered.

If, on the other hand, the computed stress is larger than σ_{pc}^{q}, then the quasi-static, scarcely viscous plastic mechanism is activated too, and the nonlinear system of four equations, consisting of Eqs. (10a, 11a) plus the following two equations (deduced from Eqs. (4a, b) and from the strain decomposition), has to be solved.

$$\exp\left(\frac{(\epsilon_{\mathrm{e}}^{i})_n+\Delta\epsilon_{\mathrm{e}}^{i}-\alpha_{\mathrm{e}}\,\epsilon_{\mathrm{e}0}}{\alpha_{\mathrm{e}}\,\kappa}\right) = \exp\left(\frac{(\epsilon_{\mathrm{p}}^{q})_n+\Delta\epsilon_{\mathrm{p}}^{q}-\alpha_{\mathrm{p}}\,\epsilon_{\mathrm{p}0}}{\alpha_{\mathrm{p}}\,(\lambda-\kappa)}\right)\left[1+\psi_{\mathrm{p}}^{q}\left(\frac{\Delta\epsilon_{\mathrm{p}}^{q}}{\Delta t}\right)\right], \tag{12a}$$

$$\Delta\epsilon=\Delta\epsilon_{\mathrm{e}}^{i}+\Delta\epsilon_{\mathrm{e}}^{v}+\Delta\epsilon_{\mathrm{p}}^{v}+\Delta\epsilon_{\mathrm{p}}^{q}, \tag{12b}$$

where $(\epsilon_{\mathrm{p}}^{q})_n$ is the quasi-instantaneous plastic strain assessed at the previous time step, and there are four unknowns involved, namely $\Delta\epsilon_{\mathrm{e}}^{i}$, $\Delta\epsilon_{\mathrm{e}}^{v}$, $\Delta\epsilon_{\mathrm{p}}^{q}$, and $\Delta\epsilon_{\mathrm{p}}^{v}$.

In all cases, the nonlinear systems of equations were solved using a conventional Newton–Rapson scheme associated with a line-search algorithm [44].

The numerical integration algorithm is summarized in Box 1. It was implemented in the Fortran User Subroutine UMAT of the commercial, finite element code ABAQUS Standard [15].

3 Typical output of the model

In this section, the different role of short- and long-term deformation mechanisms is analyzed in detail in relation to the compression behavior of fine-grained soils undergoing incremental loading (IL) oedometer tests. A sample 2 cm thick was discretized with 10 finite elements, and a fully hydromechanical coupled problem was solved (see Sect. 4 for further details). The constitutive parameters characteristic of an inorganic clay were considered.

Figure 5 shows the strain versus $\log(t)$ simulations of an oedometer testing of a soil specimen. In particular, Fig. 5a shows the typical elastic response, while Fig. 5b shows an elastoplastic response. In both cases, the short- and long-term viscous mechanisms are both activated. The output of the model is characterized by primary and secondary consolidation, the former following the typical strain–time response of Terzaghi's 1D consolidation theory, the latter represented by a near-linear plot in the $\log(t)$. The dashed lines show the two different contributions of the strain increment, namely the instantaneous short-term and the long-term viscoelastic fractions (Fig. 5a), and the quasi-instantaneous, scarcely viscous, and long-term, highly viscous, plastic fractions (Fig. 5b). Note that the evolution of the instantaneous and quasi-instantaneous strains is affected by pore pressure dissipation, while the long-term, highly viscous (elastic and plastic) deformations are governed mainly by the viscosity functions. The duration of the secondary consolidation depends on the proper calibration of the constitutive parameter $\dot{\epsilon}_{\mathrm{ref}}$: in Fig. 5 the $\epsilon^{v}-\log(t)$ plot is linear up to nearly a hundred years (for $\dot{\epsilon}_{\mathrm{ref}}=1\times10^{-10}\ \mathrm{min}^{-1}$).

Figure 5b shows that, although $\epsilon_{\mathrm{p}}^{v}$ is expected to occur earlier than $\epsilon_{\mathrm{p}}^{q}$ (because $\sigma_{\mathrm{pc}}^{v}<\sigma_{\mathrm{pc}}^{q}$), $\dot{\epsilon}_{\mathrm{p}}^{v}$ is initially almost negligible due to the high viscosity of the long-term mechanism. This is because the characteristic time related to long-term viscous phenomena is much longer than the one related to pore water dissipation in this case.

It is worth emphasizing that the short- and long-term, viscoplastic deformations are simulated by means of two

Box 1 Fully implicit algorithm for the numerical integration

Starting from the additive strain decomposition and the strain rates:

$$\Delta\epsilon^{i}_{e,n+1} + \Delta\epsilon^{v}_{e,n+1} + \Delta\epsilon^{q}_{p,n+1} + \Delta\epsilon^{v}_{p,n+1} = \Delta\epsilon_{n+1}$$

$$\dot{\epsilon}^{v}_{e,n+1} = \frac{\Delta\epsilon^{v}_{e,n+1}}{\Delta t_{n+1}},\ \dot{\epsilon}^{q}_{p,n+1} = \frac{\Delta\epsilon^{q}_{p,n+1}}{\Delta t_{n+1}},\ \dot{\epsilon}^{v}_{p,n+1} = \frac{\Delta\epsilon^{v}_{p,n+1}}{\Delta t_{n+1}}$$

1. Initialize:

$$\Delta\epsilon^{i,\text{trial}}_{e,n+1} = \Delta\epsilon_{n+1},\ \Delta\epsilon^{v,\text{trial}}_{e,n+1} = 0,\ \Delta\epsilon^{q}_{p,n+1} = 0,\ \Delta\epsilon^{v}_{p,n+1} = 0$$

2. Elastic predictor: solve the viscoelastic problem (see Eq. 10) and evaluate the *trial viscoelastic state*

from $$\left\{ \sigma^{i}_{e}\left(\Delta\epsilon_{n+1} - \Delta\epsilon^{v,\text{trial}}_{e,n+1}\right) - \sigma^{v}_{e}\left(\Delta\epsilon^{v,\text{trial}}_{e,n+1}\right) \right\} = \{0\} \qquad \text{(Box 1.1)}$$

obtain $\Delta\epsilon^{i,\text{trial}}_{e,n+1},\ \Delta\epsilon^{v,\text{trial}}_{e,n+1},\ \sigma^{\text{trial}}_{n+1}$

3. Check the viscoplastic admissibility

IF $\sigma^{\text{trial}}_{n+1} \le \sigma^{q}_{pc}$ AND $\sigma^{\text{trial}}_{n+1} \le \sigma^{v}_{pc}$

THEN $$\Delta\epsilon^{i}_{e,n+1} = \Delta\epsilon^{i,\text{trial}}_{e,n+1},\ \Delta\epsilon^{v}_{e,n+1} = \Delta\epsilon^{v,\text{trial}}_{e,n+1},$$
$$\Delta\epsilon^{q}_{p,n+1} = \Delta\epsilon^{v}_{p,n+1} = 0,\ \sigma_{n+1} = \sigma^{\text{trial}}_{n+1}$$

GOTO 7

4. Solve the long-term, viscoplastic problem (see Eq. 11)—return mapping:

from $$\left\{ \begin{matrix} \tilde{\sigma}^{i}_{e}\left(\Delta\tilde{\epsilon}^{i,\text{trial}}_{e,n+1}\right) - \tilde{\sigma}^{v}_{e}\left(\Delta\tilde{\epsilon}^{v,\text{trial}}_{e,n+1}\right) \\ \tilde{\sigma}^{i}_{e}\left(\Delta\tilde{\epsilon}^{i,\text{trial}}_{e,n+1}\right) - \tilde{\sigma}^{v}_{p}\left(\Delta\tilde{\epsilon}^{v,\text{trial}}_{p,n+1}\right) \end{matrix} \right\} = \left\{ \begin{matrix} 0 \\ 0 \end{matrix} \right\} \qquad \text{(Box 1.2)}$$

obtain $\Delta\tilde{\epsilon}^{i,\text{trial}}_{e,n+1},\ \Delta\tilde{\epsilon}^{v,\text{trial}}_{e,n+1},\ \Delta\tilde{\epsilon}^{v,\text{trial}}_{p,n+1},\ \tilde{\sigma}^{\text{trial}}_{n+1}$

5. Check the quasi-instantaneous, plastic admissibility

IF $\tilde{\sigma}^{\text{trial}}_{n+1} \le \sigma^{q}_{pc}$

THEN $$\Delta\epsilon^{i}_{e,n+1} = \Delta\tilde{\epsilon}^{i,\text{trial}}_{e,n+1},\ \Delta\tilde{\epsilon}^{v}_{e,n+1} = \Delta\tilde{\epsilon}^{v,\text{trial}}_{e,n+1},$$
$$\Delta\epsilon^{v}_{p,n+1} = \Delta\tilde{\epsilon}^{v,\text{trial}}_{p,n+1},\ \Delta\epsilon^{q}_{p,n+1} = 0,\ \sigma_{n+1} = \tilde{\sigma}^{\text{trial}}_{n+1}$$

GOTO 7.

6. Solve the complete viscoplastic problem (see Eq. 12)—return mapping:

from $$\left\{ \begin{matrix} \sigma^{i}_{e}\left(\Delta\epsilon^{i}_{e,n+1}\right) - \sigma^{v}_{e}\left(\Delta\epsilon^{v}_{e,n+1}\right) \\ \sigma^{i}_{e}\left(\Delta\epsilon^{i}_{e,n+1}\right) - \sigma^{q}_{p}\left(\Delta\epsilon^{q}_{p,n+1}\right) \\ \sigma^{i}_{e}\left(\Delta\epsilon^{i}_{e,n+1}\right) - \sigma^{v}_{p}\left(\Delta\epsilon^{v}_{p,n+1}\right) \end{matrix} \right\} = \left\{ \begin{matrix} 0 \\ 0 \\ 0 \end{matrix} \right\} \qquad \text{(Box 1.3)}$$

obtain $\Delta\epsilon^{i}_{e,n+1},\ \Delta\epsilon^{v}_{e,n+1},\ \Delta\epsilon^{q}_{p,n+1},\ \Delta\epsilon^{v}_{p,n+1},\ \sigma_{n+1}$

7. Compute the final strains

$$\epsilon^{i}_{e,n+1} = \epsilon^{i}_{e,n} + \Delta\epsilon^{i}_{e,n+1},\ \epsilon^{v}_{e,n+1} = \epsilon^{v}_{e,n} + \Delta\epsilon^{v}_{e,n+1},$$
$$\epsilon^{q}_{p,n+1} = \epsilon^{q}_{p,n} + \Delta\epsilon^{q}_{p,n+1},\ \epsilon^{v}_{p,n+1} = \epsilon^{v}_{p,n} + \Delta\epsilon^{v}_{p,n+1}$$

equivalent viscous mechanisms that are characterized by very different viscosities (using the values of the coefficients Γ^{q}_{p} and Γ^{v}_{p}): the short-term mechanism is simulated with a low viscosity, the long-term mechanism with a high viscosity. The *final stable state* of the two viscous mechanisms is reached at the same time because it depends on the constitutive parameter $\dot{\epsilon}_{ref}$, which is the same for the two mechanisms. Figure 5c shows, however, that the evolution of the quasi-instantaneous and long-term preconsolidation pressures, σ^{q}_{pc} and σ^{v}_{pc}, corresponding to Fig. 5b, is such that the steady state is practically reached much sooner for σ^{q}_{pc} than for σ^{v}_{pc} (due to the negligible slope of the curve of σ^{q}_{pc} in Fig. 5c).

4 Parametric analysis

The proposed model for 1D compression is based on 10 constitutive parameters: two parameters κ and λ for describing the slopes of the elastic and elastoplastic compression curves on a $\epsilon_v - \log\sigma_v$ plot in the *final stable state*; two partition coefficients α_e and α_p; and three parameters (Γ_e, Γ^{q}_{p}, and Γ^{v}_{p}) describing the viscous elastic and plastic strain rates. Three further parameters, $\dot{\epsilon}_{ref}$, β, and γ, define the soil's response after very long times, close to its *final stable state*. The duration of the secondary consolidation (typically expressed in thousands of years) is related to $\dot{\epsilon}_{ref}$. These latter three parameters ($\dot{\epsilon}_{ref}$, β, and γ)

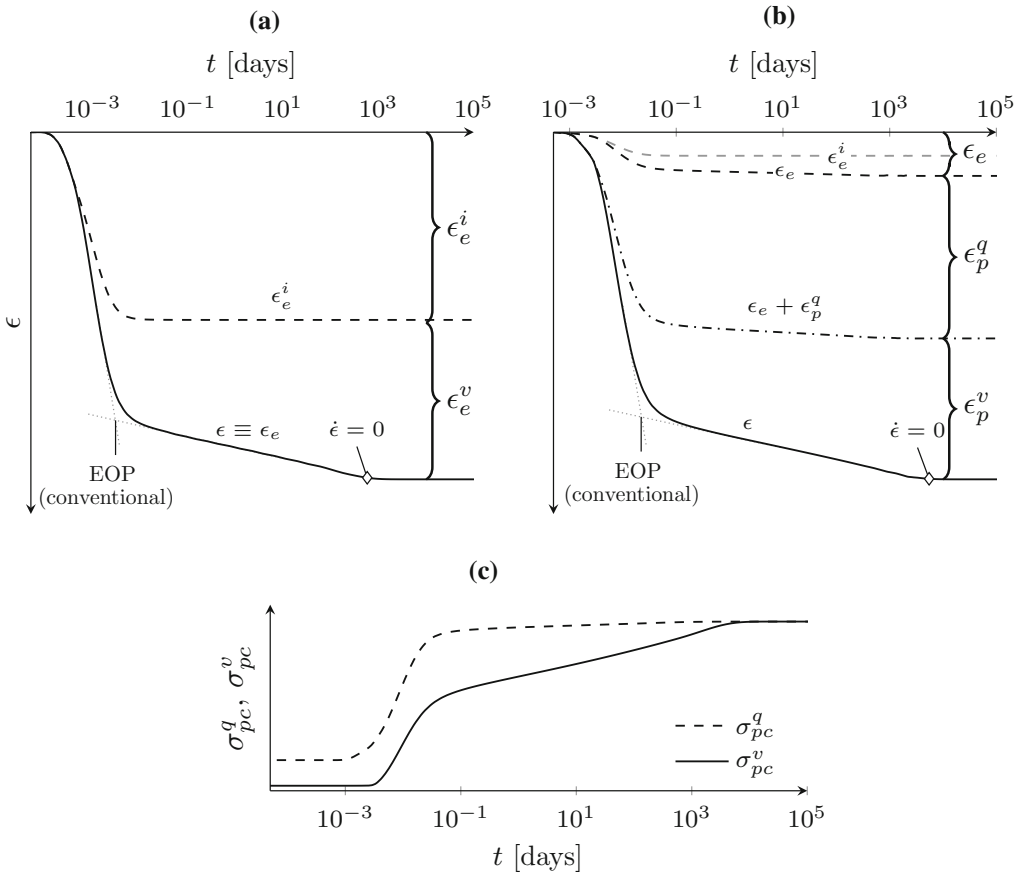

Fig. 5 Simulation of the strain–time response for a constant stress test on a thick specimen of inorganic clay. **a** Elastic load. **b** Elastoplastic load. **c** Evolution of σ_{pc} for elastoplastic load

have a minor role in the simulations, however, so their value can be chosen with a certain degree of freedom (as shown below), depending on the time scale of interest. It is only the calibration of the other seven parameters that needs to be done accurately.

In this section, the effects of each constitutive parameter are discussed in light of a parametric analysis in which each parameter is varied while the values of the others are kept constant. Reference is made to an axially symmetric sample 20 mm thick, discretized with a column of 10 uniform finite elements having a linear pore pressure (4 nodes) and quadratic solid displacements (8 nodes). The hydromechanical coupled analysis was performed with the commercial code ABAQUS [15] used to implement the proposed model. In particular, we considered the soil response induced by an instantaneous doubling of the vertical stress applied, with null transversal displacements (Fig. 6).

The parametric analyses were run assuming that the applied stresses were below the preconsolidation pressure, so the soil remained in the elastic regime ($\sigma < \sigma^v_{pc} \leq \sigma^q_{pc}$, see Fig. 3). The following analyses consequently concern the elastic parameters Γ_e, α_e, and κ, but the same observations hold for the viscoplastic regime too (for the parameters Γ^q_p, Γ^v_p, α_p, and λ) because of the structure of the model, and because the viscosity functions of the viscoplastic regime are very similar to those of the viscoelastic regime. The permeability is assumed to be $K = 8.3 \times 10^{-7}$ m/s, and a null initial strain rate is assumed as the baseline condition, $\dot{\epsilon} = 0$.

The effects induced by Γ_e on the response of the material are shown in the strain versus the logarithm of time response of Fig. 6a: for low values of Γ_e, the viscous strain very soon becomes apparent (even during primary consolidation) and the slope of the secondary phase is small. An increase in Γ_e induces a delay in the onset of viscous deformation (with an initial phase that has a negligible creep strain) and a large final slope of the secondary compression. The different curves in Fig. 6a converge on the same point (where the viscous strain rate becomes null and the *final stable state* is reached) because the same value has been assumed for $\dot{\epsilon}_{ref}$.

The effects induced by the $\dot{\epsilon}_{ref}$ parameter are shown in Fig. 6b: $\dot{\epsilon}_{ref}$ affects the duration of the viscous creep, which

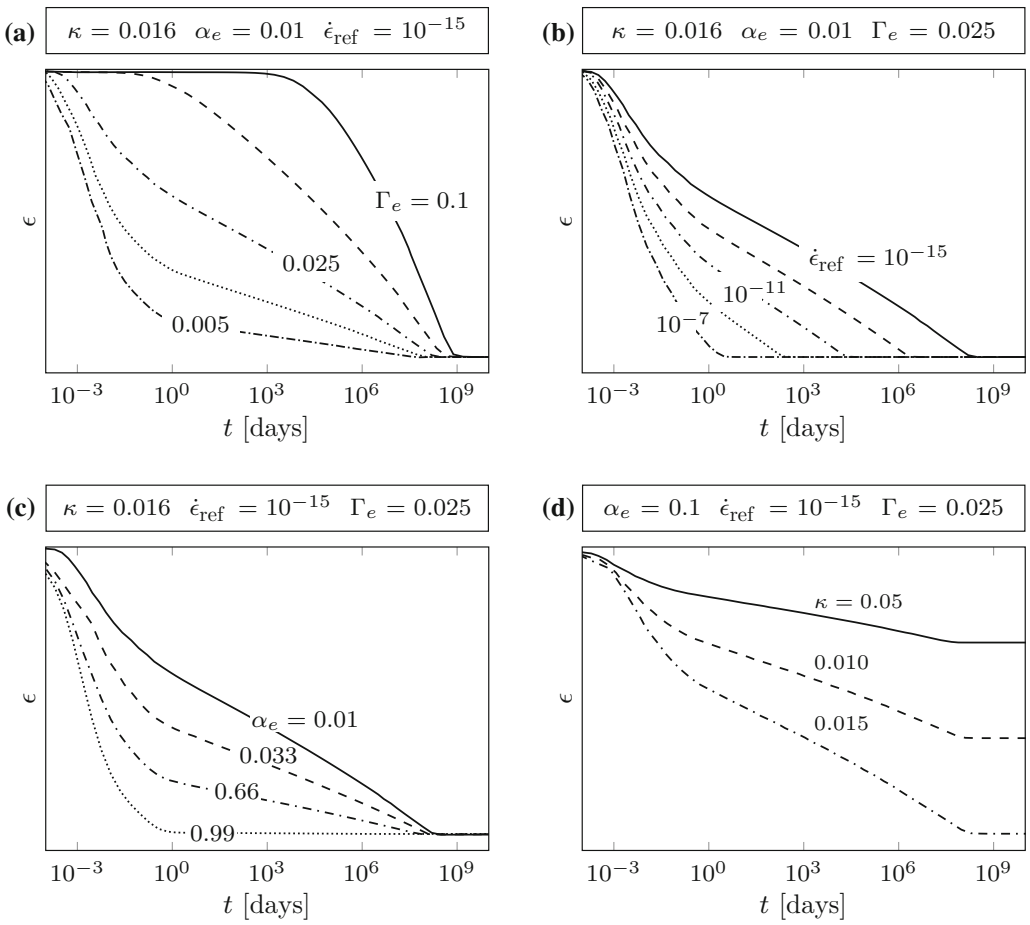

Fig. 6 Parametric analyses of constitutive model: **a** effect of Γ_e; **b** effect of $\dot{\epsilon}_{\text{ref}}$; **c** effect of α_e; **d** effect of κ (or λ)

is longer the smaller the value of $\dot{\epsilon}_{\text{ref}}$. As a result, the final parts of all the creep curves shift horizontally, while remaining parallel to one another.

Figure 6c shows the effects induced by the parameter α_e governing the separation between instantaneous and viscous deformations. This means that, if we consider the whole deformation phenomenon (up to $\dot{\epsilon} = 0$), α_e is the ratio of instantaneous to total strain in the *final stable state*. The effect induced by α_e on the global delayed response is similar to the effect of Γ_e.

Finally, the parameter κ affects the total amount of elastic strain in the *final stable state* (Fig. 6d) and has the same role as in the classical Cam–Clay theory.

5 Suggestions for calibrating the model

Here we provide some recommendations for calibrating the seven meaningful constitutive parameters of the model. Calibration should begin with the classic compressibility parameters κ and λ, which are easy to obtain from the results of a conventional oedometer test. In fact, compression curves at different strain rates keep their slopes in a $\epsilon - \log \sigma$ plot unchanged, and changes to the viscous parameters (i.e., Γ_e, α_e, Γ_p^q, Γ_p^v, α_p, and $\dot{\epsilon}_{\text{ref}}$) do not affect the slopes of the compression curves κ and λ, which can therefore be considered uncoupled from the other parameters. This model output is consistent with the conclusion reached by Laloui et al. [21] that the compression indexes do not depend on the strain rate.

The constitutive parameter $\dot{\epsilon}_{\text{ref}}$ is a scaling parameter of the strain rate defining the minimum viscous strain rate that affects the creep behavior. Figure 6b clearly shows the role of $\dot{\epsilon}_{\text{ref}}$: when the strain rate in the elastic or elastoplastic regime becomes smaller than $\dot{\epsilon}_{\text{ref}}$, the value of the viscosity function becomes negligible (Eq. 7), so the creep phenomenon practically comes to an end. This means that the $\dot{\epsilon}_{\text{ref}}$ parameter governs the duration of creep effects, the smaller the value of $\dot{\epsilon}_{\text{ref}}$, the longer it takes to reach the *final stable state*. In the range of values of interest, $\dot{\epsilon}_{\text{ref}}$ has little effect on the slope of creep deformations in a logarithm of time plot (Fig. 6b). For typical fine-grained soils, $\dot{\epsilon}_{\text{ref}}$ can be chosen in the range of 10^{-10}–$10^{-15}\,\text{min}^{-1}$, corresponding to a creep phenomenon lasting between a

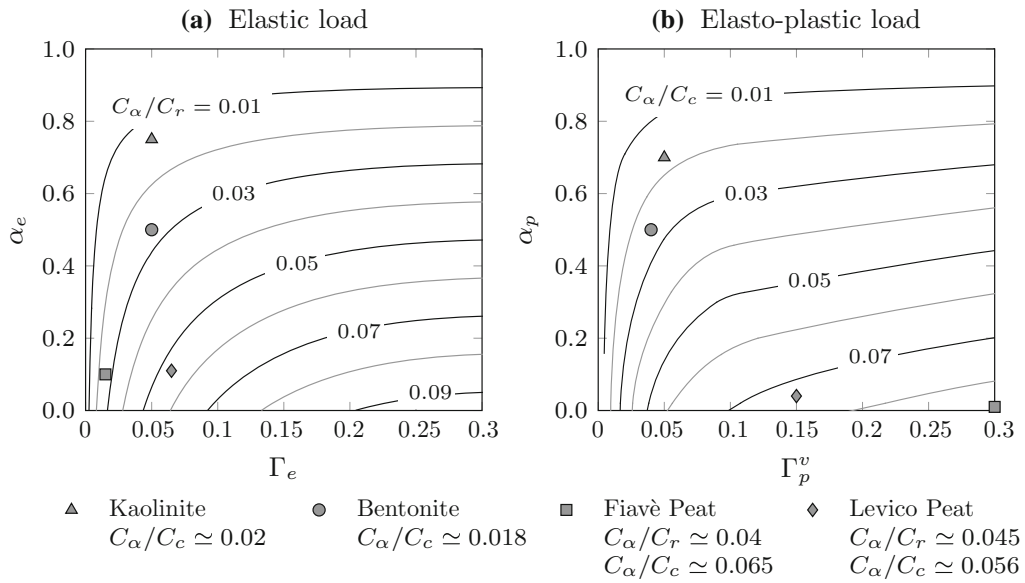

Fig. 7 Calibration chart

hundred and a million years (Fig. 5). Note that it is useful to be able to model such slow creep processes when analyzing viscous phenomena involving geological timescales.

Since the constitutive parameters β and γ affect soil response only under negligible strain rates, their effects were not explored and constant values of $\beta = 10$ and $\gamma = 1.5$ were adopted.

Defining the other parameters (α_e, α_p, Γ_e, Γ_p^q, and Γ_p^v) specifically dedicated to describing the viscous phenomena is more complicated because the effects induced by these parameters are partially interrelated, as we can see in Fig. 6a, c. Although the effects induced by the two pairs of parameters α_e–Γ_e and α_p–Γ_p^v are similar (namely a change in the slope of the creep response in the logarithm of time plot), the physical mechanisms simulated are very different, as mentioned earlier.

A first tentative assessment of α_e and α_p is conveniently based on the results of incremental loading (IL), conventional oedometer tests, considering the ratio between the deformation at the end of primary consolidation and the total deformation (after 1–2 days) for each load increment. In fact, from Fig. 1, the ratio of the intersection of the dotted line with the vertical axis (at $t = 1$ min, for instance) with respect to the total deformation (after 1–2 days) enables a first estimation of the value of α_e and α_p. Due to the previously mentioned coupling of the effects induced by $\alpha_e - \Gamma_e$ and $\alpha_p - \Gamma_p^v$, however, the subsequent refinement can only be achieved by trial and error.

Once the tentative values of α_e and α_p have been calibrated, the values of the long-term viscosities Γ_e and Γ_p^v can be selected from the slopes of the creep curves in the logarithm of time plots (namely the well-known coefficient of secondary consolidation $C_{\alpha\epsilon}$). Since the simulated slope $C_{\alpha\epsilon}$ is the outcome of both α_e and Γ_e in the elastic regime (or α_p and Γ_p^v for the plastic regime), we can plot the contours of the simulated ratio C_α/C_c (defined according to Mesri and Godlewski [35]) in a plot $\alpha_e - \Gamma_e$ (or $\alpha_p - \Gamma_p^v$ for the plastic regime), as shown in Fig. 7. These values were obtained numerically from the simulation of a load increment in a purely elastic (Fig. 7a) or an elastoplastic (Fig. 7b) regime. To obtain numerical results starting from a meaningful initial condition, each curve plotted in Fig. 7 was assessed after applying three conventional IL steps. The contour plots shown in Fig. 7 are useful for a first, tentative assessment of the constitutive parameters Γ_e and Γ_p^v.

The constitutive parameters carefully calibrated on four inorganic and organic clays with very different index properties (see Table 1) were included to validate the contours plotted in Fig. 7. The corresponding experimental values of C_α/C_r and C_α/C_c are given at the bottom of Fig. 7 and should be compared with the contour curves. A fairly good agreement exists between the experimental C_α/C_c ratios and the values expected from Fig. 7. The most notable exception concerns the elastoplastic regime of the two peats, for which the C_α/C_c ratio is probably more strongly affected by the previous stress history. Thus, although the C_α/C_c ratios shown in Fig. 7 actually depend on the whole previous stress–strain history (and are consequently only approximate), they are useful as first tentative values of Γ_e and Γ_p^v. More refined values can then be obtained by trial and error.

The typically observed range of variation of Γ_e and Γ_p^v is 0.001–0.5: the smallest values are for inorganic clays and an elastic regime.

Table 1 Calibrated constitutive parameters for the soils subjected to laboratory tests

Param.	Peat (Fiavè)	Peat (Levico) natural	Peat (Levico) Remou.	Kaolinite	Bentonite	Batiscan clay
κ	0.06	0.019	0.014	0.02	0.04	0.004
α_e	0.10	0.11	0.20	0.75	0.5	0.05
Γ_e	0.015	0.065	0.05	0.05	0.05	0.04
λ	0.30	0.112	0.122	0.07	0.14	0.38
α_p	0.01	0.04	0.20	0.75	0.5	0.05
Γ_p^q	0.03	0.015	0.015	0.005	0.005	0.004
Γ_p^v	0.30	0.15	0.15	0.05	0.05	0.04
$\dot{\epsilon}_{ref}$ (min^{-1})	10^{-10}	10^{-10}	10^{-10}	10^{-10}	10^{-10}	10^{-10}
σ_{pc}^q (kPa)	18.0	8.0	30.0	5.0	5.0	65.0
σ_{pc}^v (kPa)	4.0	4.0	19.0	5.0	5.0	65.0
K (m/s)	5×10^{-6}	5×10^{-6}	5×10^{-6}	4×10^{-7}	2×10^{-9}	8×10^{-8}

The Γ_p^q parameter describes the viscosity of the short-term, quasi-instantaneous plastic mechanism. When $\Gamma_p^q = 0$, the short-term mechanism becomes perfectly instantaneous. This parameter cannot be calibrated on oedometer test results and demands the use of triaxial tests, at least. From an analysis of the few experimental results available in the literature for inorganic clays, Madaschi and Gajo [28] concluded that $\Gamma_p^q \approx (0.05–0.10)\ \Gamma_p^v$. This parameter has a major role in the simulation of multiaxial loading conditions, but under 1D conditions it can be assumed to be null for the sake of simplicity. The interested reader can refer to [25] for a comparison of embankment settlements measured and simulated with a model based on the assumption that $\Gamma_p^q = 0$.

The initial conditions play a very important part in the proposed viscous model, especially the initial value of the preconsolidation pressures of the two viscoplastic mechanisms, σ_{pc}^q and σ_{pc}^v. These initial-state variables are related, through Eq. (5b), to the initial amounts of the viscoplastic strains, ϵ_p^q and ϵ_p^v. From a practical point of view, we have found in our simulations of undisturbed samples that σ_{pc}^q is typically quite close to the conventional preconsolidation pressure obtained from IL oedometer tests. This is reasonable because the low-viscosity mechanism practically reaches a nearly steady state in times that are extremely short from the geological standpoint.

In contrast, σ_{pc}^v is generally smaller than the conventional preconsolidation pressure and is related to the amount of initial in situ viscoplastic strain rate. As a result, if the in situ initial strain rate in soft soils has been evaluated, then σ_{pc}^v can easily be estimated from the in situ stress, using Eq. (4); or, if the initial strain rate can reasonably be assumed to be negligible, then $\sigma_{pc}^v = \sigma_{pc}^q$. If neither of the previous approaches can be applied, then an initial geological condition must be found in the recent geological history of the soil, meaning that its subsequent geological history (occurring between the chosen initial geological condition and the beginning of the engineering application) will have to be simulated to ascertain the appropriate initial conditions of the engineering problem in question. It is worth adding that, although in situ viscous strains may be negligible due to $\sigma \leq \sigma_{pc}^v = \sigma_{pc}^q$, upon reloading, both short- and long-term viscous strains are reactivated if $\sigma > \sigma_{pc}^v = \sigma_{pc}^q$. This means that the conventional preconsolidation pressure simulated by the constitutive model upon reloading generally depends on both the short- and the long-term mechanisms, for a given applied strain rate.

Finally, the initial elastic strain rate $\dot{\epsilon}_e^v$ is much more difficult to assess in soft soils, because plastic strains are predominant, whereas for stiff soils it must be established from in situ measurements and is typically expected to be negligible.

6 Comparison between model simulations and experimental results

The present model was validated against several oedometer tests performed on: two different peats (named Levico and Fiavè) with different amounts of organic content and different index properties (see [26] for a full description); two inorganic clays (industrial kaolinite and bentonite) with very different mechanical and hydraulic properties; and a natural structured clay (Batiscan clay, experimental results reported by Leroueil et al. [23]). The laboratory analyses included several types of oedometer test (incremental loading, constant rate of strain, constant rate of stress, Rowe cell MSL) adopting standard and nonstandard stress

increments and loading histories to highlight different aspects of the soils' delayed response.

The hydromechanical coupled analyses were performed with the commercial FEM code (ABAQUS, [15]) on a specimen 20 mm thick that was simulated with 10 homogeneous finite elements. The hydraulic conductivity was assumed to vary according to the Kozeny–Carman relationship, which was calibrated on the measurements obtained by Madaschi and Gajo [26].

We are aware that a rigorous analysis on oedometer test results should be performed with a multiaxial constitutive model capable of taking delayed response to vertical strains and horizontal stresses into account. Many practical engineering problems do not require such a complex approach, however, because the information provided by a simple 1D model suffices. A simple 1D approach may also provide useful insight for the formulation of a fully multiaxial constitutive framework, taking viscous deformation into account.

Calibration of the constitutive parameters was based on the suggestions in Sect. 5. Table 1 shows the calibrated values that provided the global best fit for the six different soils considered. Note that the σ^q_{pc} of natural Levico Peat is much smaller than that of the remolded sample because the former was collected at a very shallow depth, while the latter was initially consolidated in a large oedometer cell starting from a slurry. The values of the hydraulic conductivity given in Table 1 refers to the beginning of the tests. Destructuring phenomena were deliberately neglected in this work, however.

It is worth noting that the peaty soils' behavior is dominated by the viscous strain, so the partition coefficients α_e and α_p are very small by comparison with inorganic soils, whereas the viscous coefficient Γ^v_p is much larger than for inorganic soils.

6.1 Simulation of the IL oedometer tests

When a large load increment is applied to an inorganic clay sample undergoing a conventional oedometer test, the evolution of the settlements follows a classic S-shaped curve in a strain versus logarithm of time plot, from which the end of primary consolidation (EOP) is easy to estimate using the Casagrande graphical method. In contrast, the evolution of the settlements of peaty soils is typically less curved and the 'S' shape is missing, making it generally difficult to identify the EOP.

The proposed constitutive model can simulate both kinds of behavior appropriately, as shown in Fig. 8, where the simulations and experimental results obtained for the two inorganic clays and the peats are compared. In particular, the plots on the left show the oedometric compression curves, while those on the right show some $\epsilon - \log t$ steps.

It is worth emphasizing that the constitutive parameters were calibrated taking the full loading history into account, and striving to obtain the best fit in all the loading steps, so certain compromises had to be made. A better simulation could have been obtained if the stress history to simulate had been less broad and complicated than the one considered here. The agreement between the simulations and the measurements is excellent nonetheless, in terms of both compression curves and the evolution of the deformations.

It is well known [36, 37] that the delayed behavior of soils is strongly influenced by the load increment ratio. In particular, applying small load increments initially induces negligible primary and secondary settlements, then the slope of the $\epsilon - \log t$ curves in the secondary phase increases considerably [26, 36]. The delayed response induced by small load increments is of interest in many engineering applications (e.g., releveling road embankments after settlement), and that is why it is important to validate the reliability of the proposed constitutive model under this type of loading condition.

To do so, it is convenient to introduce the concept of effective surcharge ratio $R'_s = \sigma'_{vf}/\sigma'_{vi} - 1$ [34], where σ'_{vi} and σ'_{vf} represent the effective vertical pressure at the start and end of the loading increment, respectively.

Figure 9 shows the comparison between the simulations and the measurements obtained from small loading and unloading steps on Fiavè peat [26]. The results are plotted in a $\epsilon - \log t$ plot. The constitutive model correctly simulates the creep curves induced by small load increments ($R'_s \gtrsim 0$), including the previously mentioned negligible primary compression and the continuous increase in the slope for the secondary compression.

The delayed response of peaty soils after small unloading steps ($R'_s \lesssim 0$) is rather unexpected because an initial phase of delayed swelling is followed by a second phase of delayed compression. This type of response is of interest in the case of preloading embankments, for instance, and was first highlighted by Samson and La Rochelle [46] in organic soils, though it is typically seen in inorganic clays too [32, 34]. The excellent consistency between our model simulations and the measurements obtained on Fiavè peat is shown in Fig. 9.

6.2 Quasi-preconsolidation effect

The quasi-preconsolidation effect induced by aging is a well-known aspect of the rheological behavior of fine-grained soils. This effect was first observed by Leonards and Ramiah [22], then analyzed by Bjerrum [4], and later confirmed by many others (e.g., [33]).

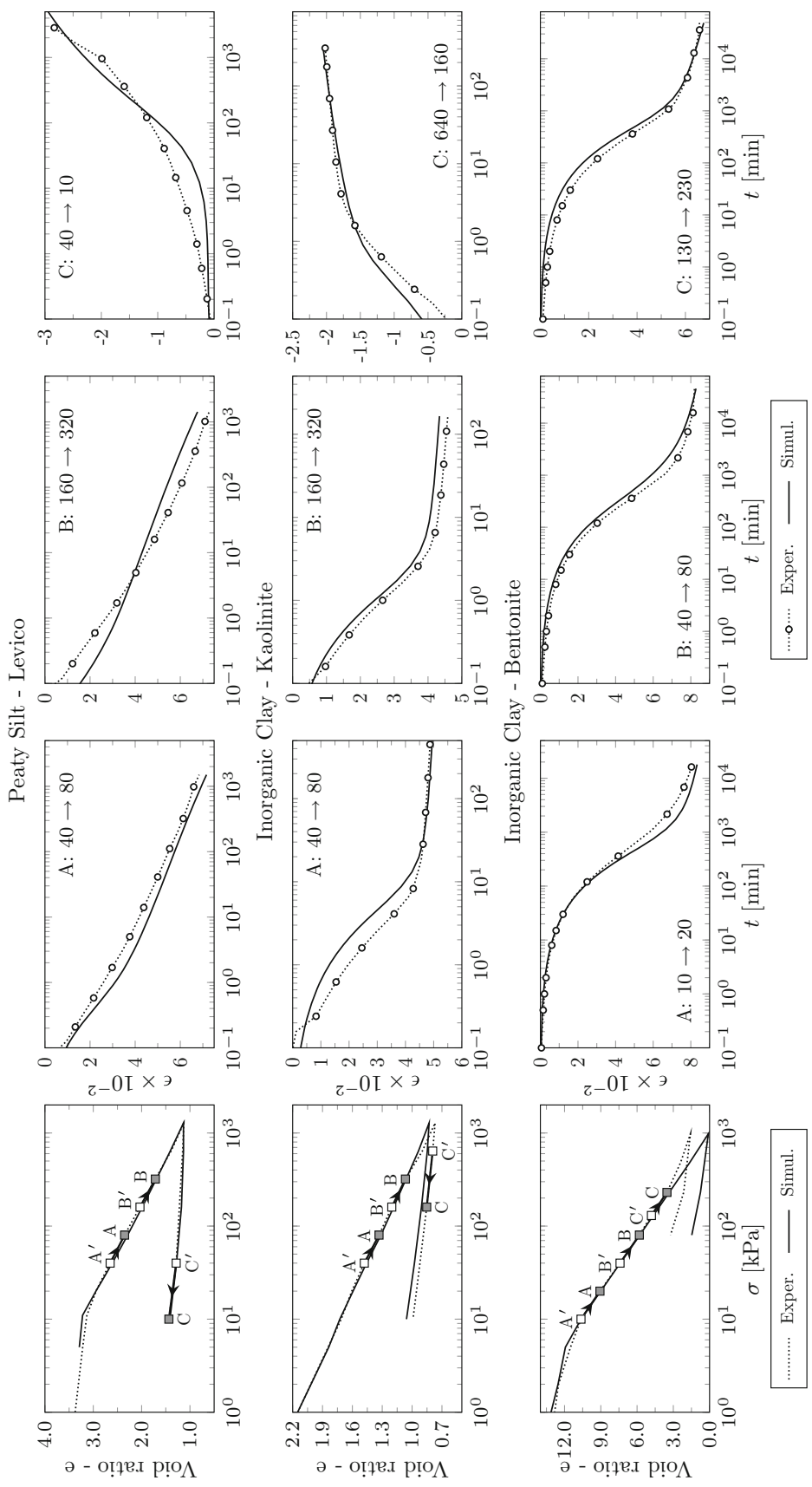

Fig. 8 Simulation of peaty soils and inorganic clays behavior

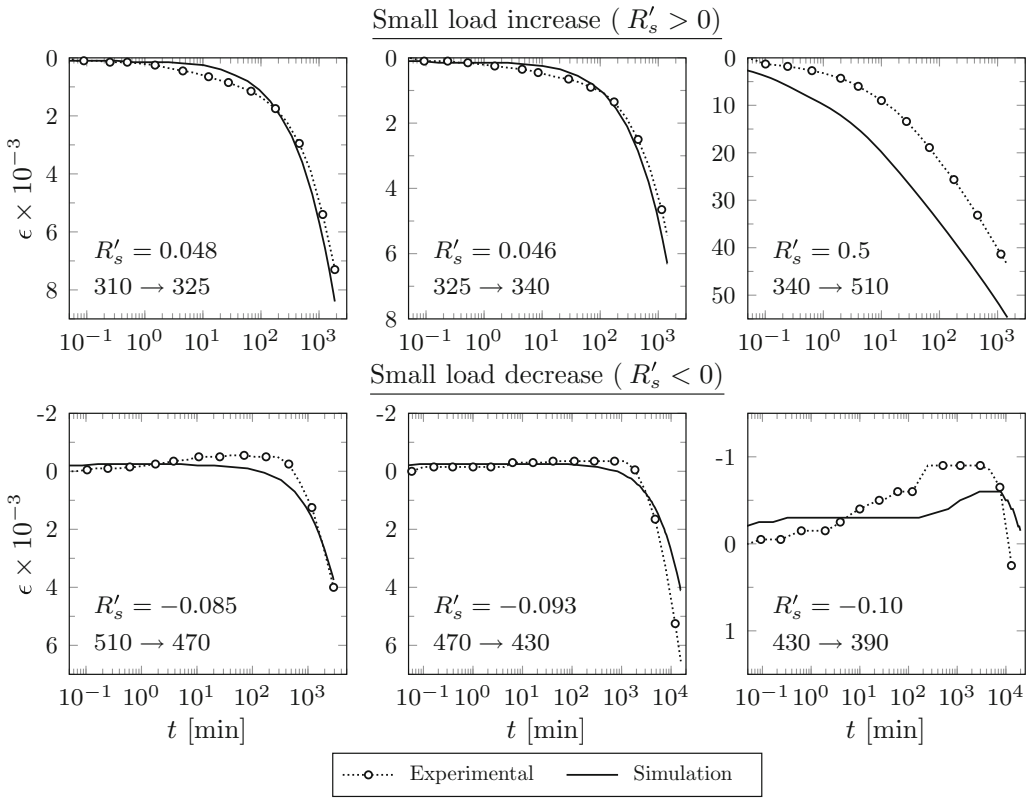

Fig. 9 Small loading and unloading on Fiavè Peat [26]: experiment versus simulation

Madaschi and Gajo [26] analyzed the quasi-preconsolidation induced by aging in Fiavè peat using IL oedometer tests. After initial loading, the sample was kept under a constant vertical stress of 160 kPa for 30 days, and then the loading process was resumed, applying small load increments (about $R'_s = 0.08$), each lasting 24 h. As shown in Fig. 10, the resulting quasi-preconsolidation pressure induced by 30-day aging was about 250 kPa. The excellent agreement between our model simulations and these experimental results is shown in Fig. 10.

It is worth adding that for peats, the simulated quasi-preconsolidation effect turned out to be scarcely affected by the short-term viscous mechanism (in fact, the instantaneous-viscous, IV model proposed by Madaschi and Gajo [27], provided a similar quasi-preconsolidation pressure to the one predicted by the present viscous-viscous, VV model). This means that the quasi-preconsolidation effect is mostly due to the long-term, viscoplastic mechanism, at least for peats and inorganic soils.

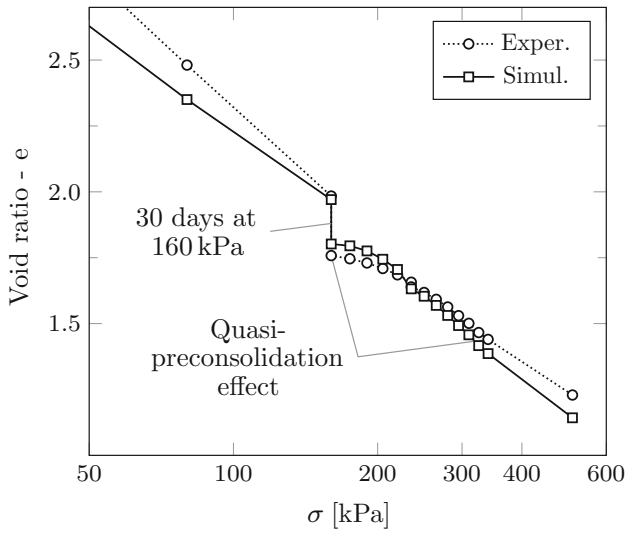

Fig. 10 Simulation of quasi-preconsolidation effect for Fiavè peat (specimen A)

6.3 Constant rate of strain (CRS) oedometer tests

Constant rate of strain (CRS) oedometer tests [13, 23] enable a rapid assessment of the 1D compressibility of soils, in which the delayed soil response may have important effects, however. Simulations obtained with the model were compared with experimental results obtained by Leroueil et al. [23] on conducting CRS tests on natural Batiscan clay.

The constitutive parameters of the model were first calibrated on the incremental loading (IL) creep tests performed by Leroueil et al. [23] on Batiscan clay, as given in

Table 1. The excellent consistency between the simulations and the measurements obtained from the IL creep tests is apparent in Fig. 11. The same values of the constitutive parameters calibrated on the IL tests (in Table 1) were then used to simulate the CRS tests conducted by Leroueil et al. [23], which involved a very wide range of strain rates. As a result, the simulations shown in Fig. 12 should be intended as model predictions. The greatest strain rate employed in the tests sufficed to ensure a full dissipation of the pore pressures (see Fig. 1 in [23]). This is consistent with the simulations (Fig. 11) which provide a maximum pore pressure excess of 0.1 kPa, under approximately a vertical load of 150 kPa, for the greatest strain rate of $10^{-6}\,s^{-1}$. Equivalently, Fig. 13 shows the comparison between the model predictions and the measurements obtained by means of a special CRS conducted by Leroueil et al. [23], by changing the strain rate during the loading (leading in any case to a negligible excess pore pressure within the sample).

The results shown in Figs. 11, 12, and 13 demonstrate the general agreement between the simulations and the experimental results. In particular, the constitutive model accurately simulates the differences between the delayed response induced by large stress increments (for which the strain-log t curves have the typical 'S' shape) and those induced by small stress increments (presenting stress–strain curves with a continuous slope increment), as shown in Fig. 11.

The main inconsistency concerns the simulated compression stress–strain curves obtained in CRS tests, which have a constant slope (in a strain versus logarithm of stress plot, Figs. 12, 13), unlike the curved lines obtained with the measurements, which have an upward concavity (i.e., a decrease in the slope at the higher applied stresses) related to destructuring phenomena in this highly structured, natural clay. Destructuring phenomena could easily be taken account by incorporating a new internal variable describing the amount of *structure* that either undergoes an

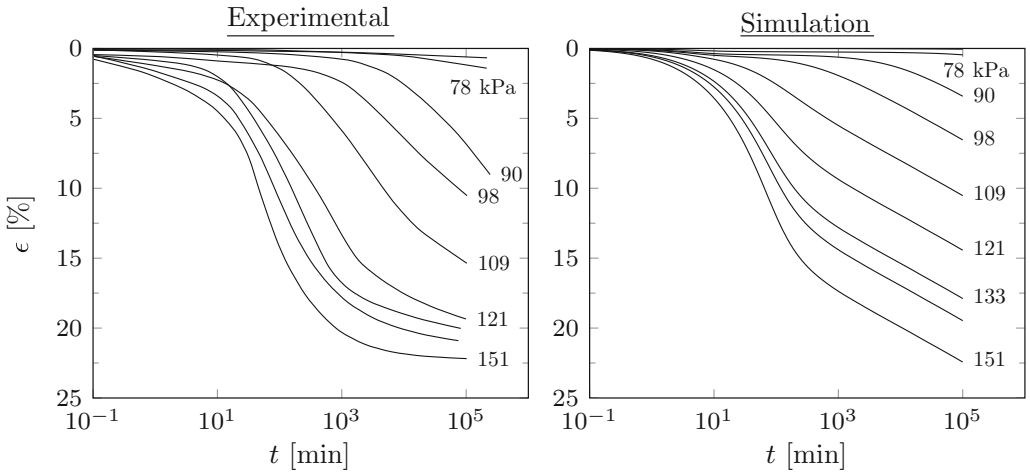

Fig. 11 Simulation of creep oedometer tests on Batiscan clay [23]

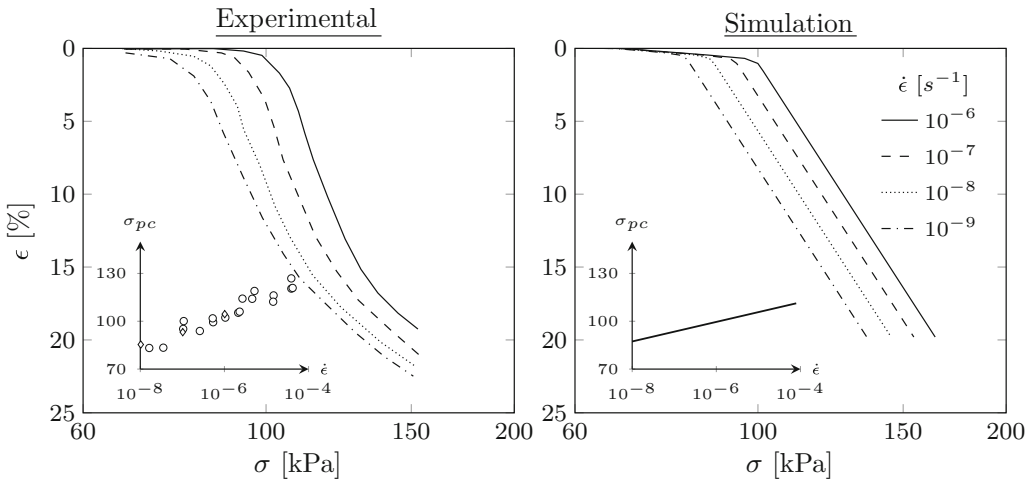

Fig. 12 Simulation of constant rate of strain oedometer tests on Batiscan clay [23]

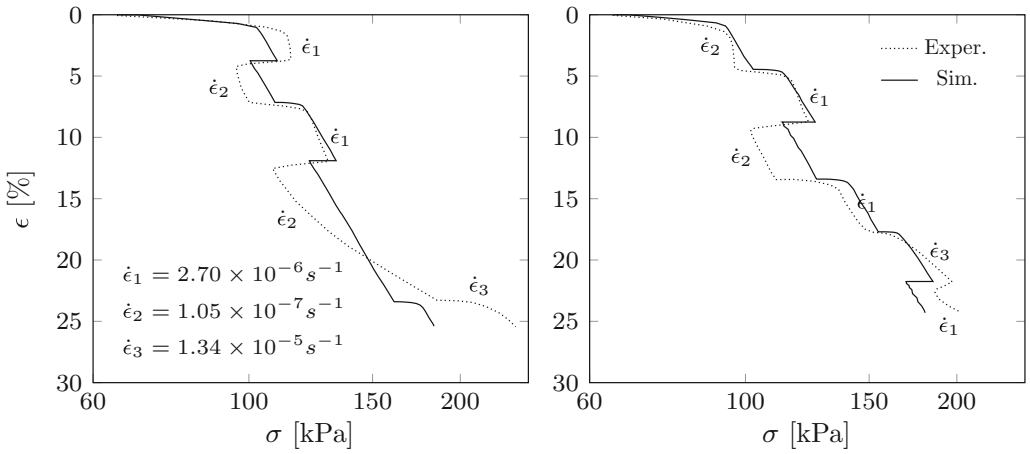

Fig. 13 Simulation of CRS oedometer tests at variable strain rates, on Batiscan clay [23]

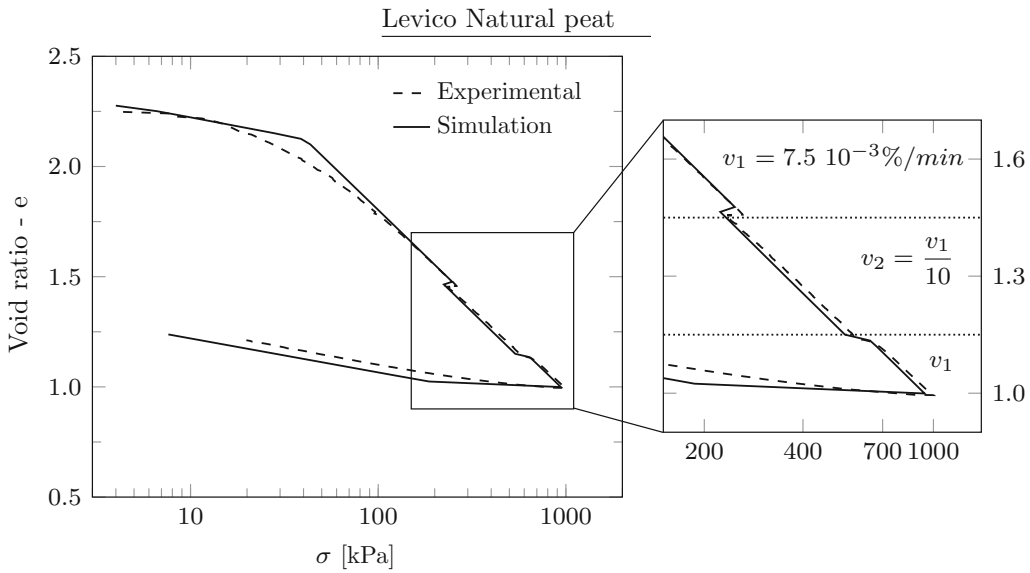

Fig. 14 Simulation of constant rate of strain (CRS) test on Levico natural peat

exponential decay as a result of the accumulation of plastic strains (see [12], for inviscid structured soils, and [20], for viscous ones), or increases due to the deposition of cementation bonds [11].

Some discrepancies between the model's simulations and the experimental results in Fig. 13 are certainly related to destructuring phenomena, but a part of the discrepancies might be intrinsic in the isotache concept and further experimental results would be needed.

The output of the model for CRS tests was also compared with experimental results obtained for peaty soils (Levico peat, tested by Madaschi and Gajo [26]). The constitutive parameters were calibrated in the same way as for the IL tests described in Sect. 6.1. The sample was initially loaded at a strain rate of 7.5×10^{-3} %/min; then, under a vertical effective stress of 260 kPa, the strain rate was reduced to 7.5×10^{-4} %/min and kept constant up to a vertical stress of 580 kPa. The initial strain rate of 7.5×10^{-3} %/min was then resumed until the end of the test. Figure 14 shows the comparison between the simulations and the experimental results. The model correctly predicts the effects induced by the abrupt change in the strain rate applied.

6.4 Constant rate of stress (CRSS) oedometer tests

While CRS oedometric tests are quite widely used, constant rate of stress oedometer tests (CRSS) are rarely adopted because they involve a more complex experimental setup and rely on a computer-controlled pneumatic piston. The advantage of this type of test lies, however, in that it enables a model's response to load reversals to be

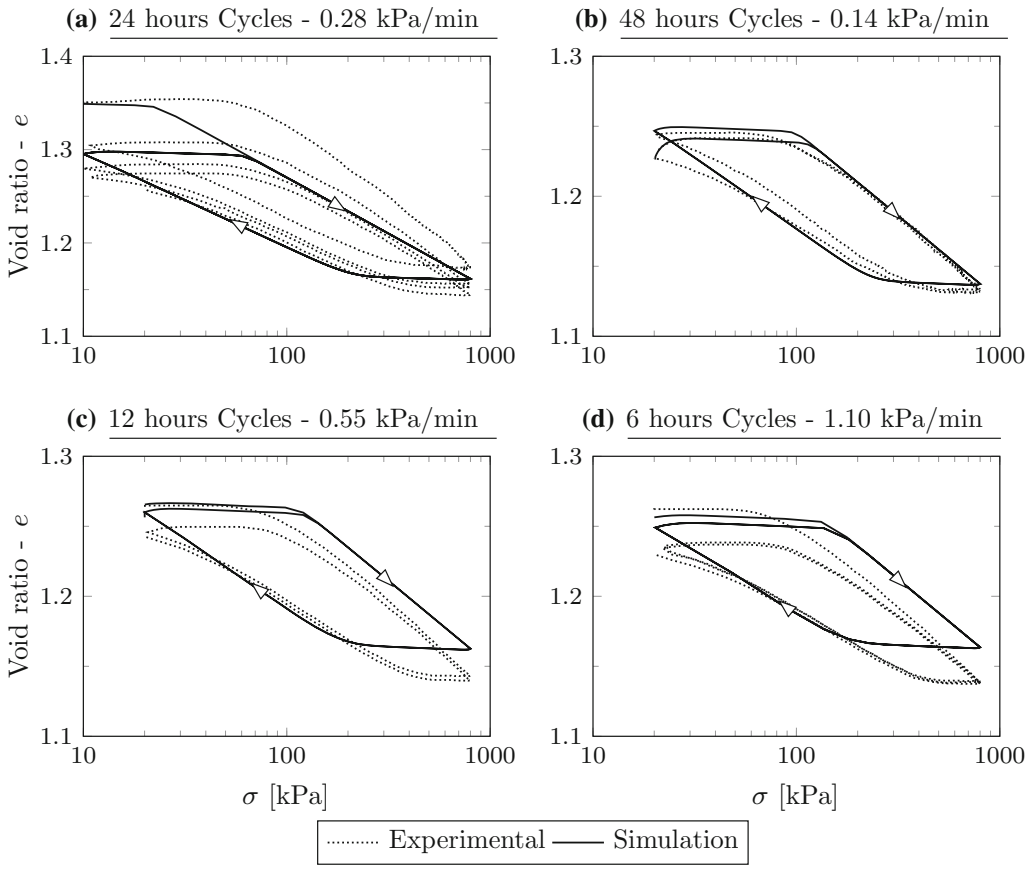

Fig. 15 Simulation of CRSS tests for Levico peat (specimen A) [26]

validated. In fact, the general soil response measured in CRSS tests is fairly similar to that of CRS tests—except for the load reversals, as shown below.

It is worth adding here that, despite its importance in geotechnical engineering applications, delayed soil behavior under unloading–reloading cycles has rarely been the object of experimental investigations [1, 18, 19]). That is why the unloading–reloading CRSS tests performed on Levico peat by Madaschi and Gajo [26] were considered here. A peat sample was first loaded and unloaded in a standard IL test, and then it was submitted to several reloading–unloading CRSS cycles using different stress rates. The load–unload cycles ranged between 10–20 and 800 kPa. The constant stress rate applied was in the range of 0.14 kPa/min (load cycle lasting 48 h) and 1.10 kPa/min (load cycle lasting 6 h), which led to the formation of negligible excessive pore pressures. The first CRSS cycles applied are those of Fig. 15a, while the last are shown in Fig. 15d.

In Fig. 15, the laboratory results are compared with the simulations, showing a very good agreement in terms of the amplitude of the hysteresis loops and the amount of deformation. It is worth noting the excellent consistency between the model's output and the measurements already in the first reloading phase (Fig. 15a).

It is worth adding that the computed delayed behavior in Fig. 15 is due partly to a viscoplastic mechanism and partly to viscoelasticity. The former is expected to still be active in Fig. 15a (concerning the CRSS results obtained first, after the mechanical IL unloading) and to become less and less relevant moving toward Fig. 15d (which shows the results obtained after many CRSS unload–reload cycles). As a result, the evolution of discrepancies between model simulations and experimental results, moving from Fig. 15a, d, can be partly attributed to a progressive fading of the viscoplastic effects. The slightly greater ratcheting (in the first cycle) of the experiments with respect to the simulations (in Fig. 15c, d) probably means that the viscoelastic model needs some improvement, in its calibration at least. Be that as it may, it is worth noting that many aspects of the experimental results are well captured, in qualitative terms at least: see, for instance, the fact that the first reloading path in Fig. 15c, d is slightly higher than the later ones. This effect is due entirely to a change in the stress rate applied in a given set of CRSS cycles with respect to the previous one.

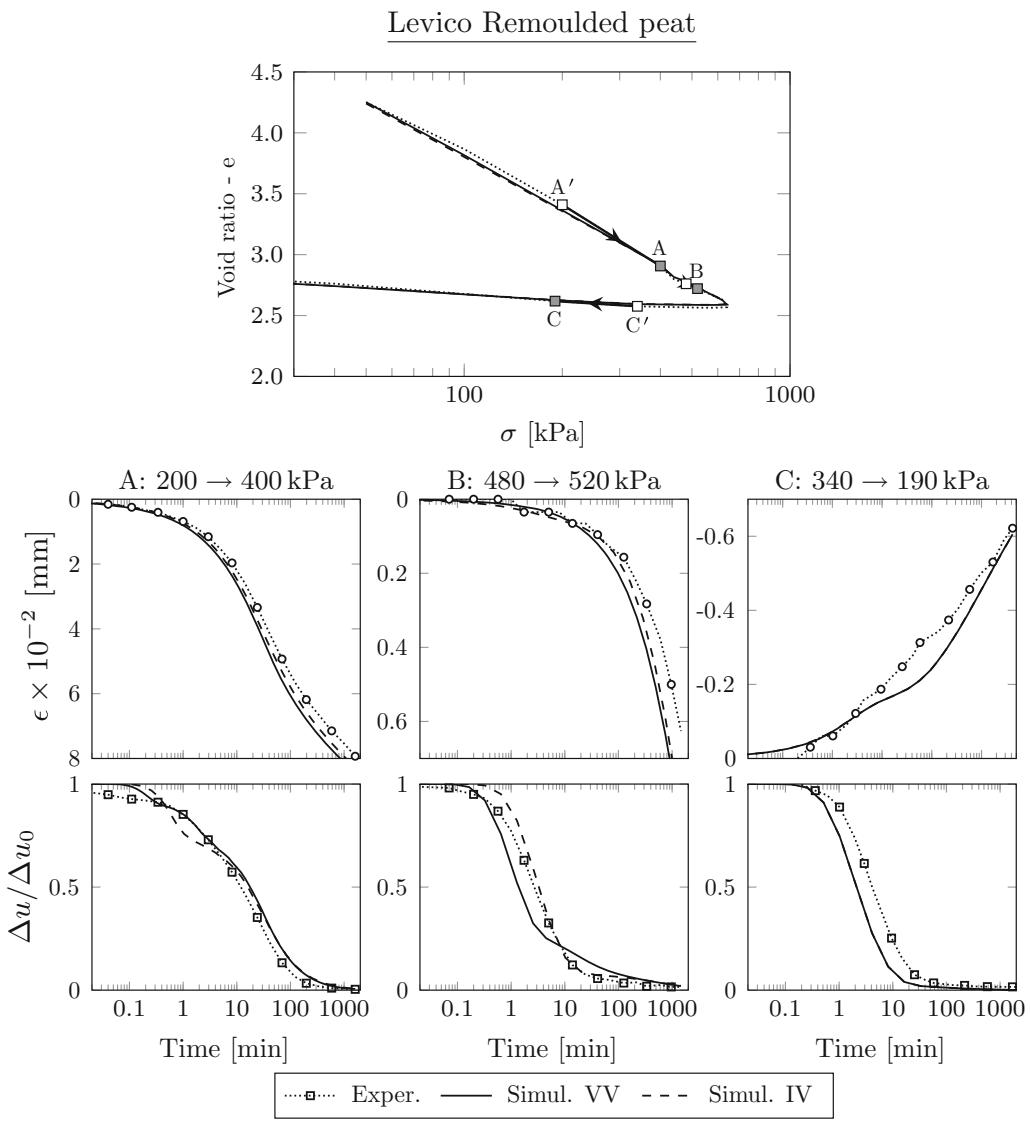

Fig. 16 Simulation Rowe cell test on Levico remolded peat

The slope of the nearly horizontal parts of the curves in Fig. 15 depends on the α_e, so its negligible inclination is consistent with the small value of α_e chosen for these organic clays (see Table 1). The extension of the nearly horizontal parts of the curves depends mainly on Γ_e.

6.5 Rowe cell oedometer tests

The simulations obtained with the model were also compared with the pore pressure and vertical displacements measured by Madaschi and Gajo [26] with a small Rowe consolidation cell. The experiments were conducted on a remolded specimen of Levico peat. The sample was first saturated using an appropriate back pressure, and then it was submitted to a conventional IL test, in which drainage was only permitted from the top of the specimen, whereas pore pressure was measured at the bottom.

Figure 16 shows the evolution of the vertical strains and excess pore pressures measured under three load increments. The simulations are compared with the experimental measurements in Fig. 16. The calibrated values of the constitutive parameters are given in Table 1 and differ slightly from those used for the simulations discussed in the previous subsections (referring to natural peats) because this is a remolded soil.

For the sake of completeness, Fig. 16 shows the results obtained with the [IV] viscoplastic model (with $\Gamma_p^q = 0$ and $\alpha_p = 0.04$) as compared with the results of the [VV] viscoplastic model (with $\Gamma_p^q = 0.015$ and $\alpha_p = 0.20$, Table 1). Note that measuring pore pressure dissipation during

primary consolidation could be considered a possible method to analyze the characteristics of short-term mechanisms, which are typically hidden by primary consolidation. Figure 16 shows, however, that both formulations provide very consistent simulations for both large load increments (i.e., 200 → 400 kPa) and small load increments (i.e., 480 → 520 kPa). We surmise that it is impossible to establish from the strain and pore pressure evolutions measured in the Rowe consolidation cell which viscoplastic model (either [IV] or [VV]) is the most suitable for simulating the experimental results. This information can only be obtained by combining the oedometer and multiaxial test results [28].

A very good consistency between the modeled and experimental results emerges in Fig. 16 for unloading too (i.e., 340 → 190 kPa), in terms of both vertical strain history and pore pressure evolution at the bottom of the sample. This consistency highlights the reliability of the assumed elastic and viscoelastic mechanisms.

Finally, Fig. 16 shows that monitoring pore pressure evolution during primary consolidation in addition to settlement evolution generally enables a much more accurate model calibration than simply analyzing settlement evolution.

7 Conclusions

The 1D, viscoelastic and viscoplastic model proposed here is based on a logarithmic viscosity function used within Perzyna's framework. The specially adapted logarithmic viscosity function accurately simulates the isotache concept first proposed by Suklje [47] and later extended by Bjerrum [4]. At first sight, our model could therefore be considered an in-depth and rigorous validation of the isotache concept.

The proposed model is not merely an implementation of the isotache concept, however. The work explores in detail the need to consider two deformation mechanisms with two different velocities, which are implemented for the first time within Perzyna's theory, by using two yield stresses. One is a short-term mechanism (considered here as an instantaneous mechanism, for the elastic behavior, and as a scarcely viscous mechanism, for the plastic response); the other is a long-term, highly viscous mechanism (for both elastic and plastic deformations). The two mechanisms contribute in different proportions to the final response of fine-grained soils: the short- and long-term mechanisms have much the same amplitude in inorganic clays, while in peats the short-term mechanism is vanishingly small by comparison with the long-term one.

The proposed model proved capable of simulating the most important aspects of the soils' delayed response under a variety of loading and unloading conditions.

The key ingredients of our model include the breakdown of the strain into four components (the elastic and plastic, instantaneous and viscous fractions, according to Eq. 1), and a specially adapted logarithmic viscosity function (Eq. 7). In particular, the delayed behavior is found to depend on both the strain amplitude and the strain rate, ϵ and $\dot{\epsilon}$. These ingredients enable an accurate simulation of the major features of the viscous response over a wide range of fine-grained soils (from inorganic to highly organic clays and peats) under a wide range of 1D loading and unloading conditions. The model was validated over a very ample range of loading conditions (incremental loading creep tests, under both very small and very large load increments/decrements, constant rate of strain tests and constant rate of stress tests), considering a broad array of applied stress and strain rates, and including a comparison with calculated and measured pore pressure dissipations.

Acknowledgements The authors gratefully acknowledge Financial Support from European Union FP7, Project under Contract Number PIAPP-GA-2013-609758-HOTBRICKS.

Appendix

The polynomial coefficients a, b, and c of the viscosity function given in Eq. (7) depend on two parameters, β and γ, which define the position of the transition point (between the logarithmic and polynomial branches) and the tangent of the viscosity function at the origin of the axis (see Fig. 4).

The coefficients were simply obtained by imposing the smooth continuity of the function at the transition point:

$$a = \frac{\gamma \ \log \beta}{\beta \, \dot{\epsilon}_{\mathrm{ref}}} \tag{13a}$$

$$b = \frac{3 \log \beta - 2 \ \gamma \ \log \beta - 1}{\left(\beta \, \dot{\epsilon}_{\mathrm{ref}}\right)^2} \tag{13b}$$

$$c = \frac{\gamma \ \log \beta + 1 - 2 \log \beta}{\left(\beta \, \dot{\epsilon}_{\mathrm{ref}}\right)^3} \tag{13c}$$

References

1. Acosta-Martinez H, Tatsuoka F, Li JZ (2005) Viscous property of clay in 1-D compression: evaluation and modelling'. In: Proceedings 16th ICSMGE, Osaka, pp 779–783
2. Adachi T, Oka F (1982) Constitutive equations for normally consolidate clay based on elasto-viscoplasticity. Soils Found 22(4):57–70
3. Berre T, Nersen K (1972) Oedometer tests with different specimen heights on a clay exhibiting large secondary compression. Géotechnique 22(1):53–70

4. Bjerrum L (1967) Engineering geology of norwegian normally-consolidated marine clays as related to settlements of buildings. Géotechnique 17(2):83–118
5. Borja RI, Choo J (2016) Cam–Clay plasticity. Part VIII: A constitutive framework for porous materials with evolving internal structure. Comput Methods Appl Mech Eng 309:653–679. ISSN: 00457825
6. Borja RI, Kavazanjian E (1985) A constitutive model for the stress–strain–time behaviour of 'wet' clays. Géotechnique 35(3):283–298
7. Cosenza P, Korosak D (2008) Secondary consolidation of clay as an anomalous diffusion process. Int J Numer Anal Methods Geomech 32:189–213
8. Di Benedetto H, Tatsuoka F, Ishihara M (2002) Time-dependent shear deformation characteristics of sand and their constitutive modelling. Soils Found 42(2):1–22. ISSN: 09168451
9. Fodil A, Aloulou W, Hicher PY (1997) Viscoplastic behaviour of soft clay. Géotechnique 47(3):581–591
10. Fox PJ, Edil TB, Lan LT (1992) C_α/C_c concept applied to compression of peat. J Geotech Eng 118(8):1256–1263
11. Gajo A, Cecinato F, Hueckel T (2015) A micro-scale inspired chemomechanical model of bonded geomaterials. Int J Rock Mech Min Sci 80:425–438. ISSN: 13651609
12. Gajo A, Muir Wood D (2001) A new approach to anisotropic, bounding surface plasticity: general formulation ad simulation of natural and reconstituted clay behaviour. Int J Numer Anal Methods Geomech 25:207–241
13. Gorman CT et al (1978) Constant-rate-of-strain and controlled-gradient consolidation testing. Geotech Test J 1(1):3–15
14. Haupt P (2002) Continuum mechanics and theory of materials. Springer, Berlin
15. Hibbitt D, Karlsson B, Sorensen P (2009) ABAQUS standard user's manual, version 6.9-EF. Hibbitt, K., Pawtucket
16. Hinchberger SD, Rowe RK (2005) Evaluation of the predictive ability of two elastic-viscoplastic constitutive models. Can Geotech J 42(6):1675–1694
17. Kaliakin VN, Dafalias YF (1990) Theoretical aspects of the elastoplastic–viscoplastic bounding surface model for cohesive soils. Soils Found 30(3):11–24
18. Kawabe S, Kongkitkul W, Tatsuoka F (2011) 1D compression with unload/reload cycles on soft clay and its simulation. In: Proceedings of 14th Asian Regional conference on SMGE, Hong-Kong
19. Kawabe S, Tatsuoka F (2013) Creep characteristics of clay in one-dimensional compression with unloading/reloading cycles. In: 18th international conference on soil mechanics and geotechnical engineering. Leroueil, pp 235–238
20. Kimoto S, Oka F (2005) An elasto–viscoplastic model for clay considering destructuralization and consolidation analysis of unstable behavior. Soils Found 45(2):29–42
21. Laloui L, Leroueil S, Chalindar S (2008) Modelling the combined effect of strain rate and temperature on one-dimensional compression of soils. Can Geotech J 45(12):1765–1777
22. Leonards GA, Ramiah BK (1960) Time effects in the consolidation of clays. In: ASTM STP 254. ASTM, Philadelphia, pp 116–130
23. Leroueil S et al (1985) Stress–strain–strain rate relation for the compressibility of sensitive natural clays. Géotechnique 35(2):159–180. ISSN: 0016-8505
24. Liingaard M, Augustesen A, Lade PV (2004) Characterization of models for time-dependent behavior of soils. Int J Geomech 4:157–177
25. Madaschi A, Gajo A (2015a) Constitutive modelling of viscous behaviour of soils: a case study. Geomech Energy Environ. ISSN: 23523808
26. Madaschi A, Gajo A (2015b) One-dimensional response of peaty soils subjected to a wide range of oedometric conditions. Géotechnique 65(4):274–286
27. Madaschi A, Gajo A (2016a) A two-yield surfaces, viscoplastic constitutive model for ceramics and geomaterials. J Eur Ceram Soc (**in press**). ISSN: 09552219
28. Madaschi A, Gajo A (2016b) A viscoplastic double yield surface constitutive model for geologic materials. In: In preparation
29. Malvern LE (1951) The propagation of longitudinal waves of plastic deformation in a bar of material exhibiting a strain-rate effect. J Appl Mech 118:203–208
30. Maranha JR, Pereira C, Vieira A (2016) A viscoplastic subloading soil model for rate-dependent cyclic anisotropic structured behaviour. Int J Numer Anal Methods Geomech 40:1531–1555. ISSN: 03639061. arXiv: nag.2347[10.1002]
31. Mesri G (1973) Coeffcient of secondary compression. J Soil Mech Found Div ASCE 99(SM1):123–137
32. Mesri G, Ajlouni M (2007) Engineering properties of fibrous peats. J Geotech Geoenviro Eng 133:850–866
33. Mesri G, Castro A (1987) C_α/C_c concept and K0 during secondary compression. J Geotech Eng 113(3):230–247
34. Mesri G, Feng TW (1991) Surcharging to reduce secondary settlements. In: Proceedings, international conference on geotechnical engineering for coastal development. Theory to Practice, Yokohama, Japan, pp 359–364
35. Mesri G, Godlewski PM (1977) Time and stress-compressibility interrelationship. J Geotech Eng Div 103(5):417–430
36. Mesri G, Lo DOK, Feng TW (1994) Settlement of embankments on soft clays. In: ASCE specialty conference—Geotechnical Special Publication, vol 40, number 1, pp 8–56
37. Mesri G, Stark TD, Ajlouni M et al (1997) Secondary compression of peat with or without surcharging. J Geotech Geoenviron Eng 123(5):411–0421
38. Mesri G, Stark TD, Chen CS (1994) C_α/C_c concept applied to compression of peat—discussion. J Geotech Eng 120(4):764–767
39. Naghdi PM, Murch SA (1963) On the mechanical behaviour of viscoelastic/plastic solids. J Appl Mech 30(3):321–328
40. Navarro V, Alonso EE (2001) Secondary compression of clays as a local dehydration process. Géotechnique 51(10):859–869
41. Perzyna P (1963a) The constitutive equations for rate sensitive plastic materials. Q Appl Maths 20(4):321–332
42. Perzyna P (1963b) The constitutive equations for work-hardening and rate sensitive plastic materials. In: Proceedings of vibration problems, pp 281–290
43. Perzyna P (1966) Fundamental problems in viscoplasticity. Adv Appl Mech 9:244–368
44. Press WH et al (2001) Numerical recipes in Fortran 77: the art of scientific computing. Cambridge University Press, Cambridge
45. Qiao Y et al (2016) Nonstationary flow surface theory for modeling the viscoplastic behaviors of soils. Comput Geotech 76:105–119. ISSN: 0266-352X
46. Samson L, La Rochelle P (1972) Design and performance of an expressway constructed over peat by preloading. Can Geotech J 9:447–466
47. Suklje L (1957) The analysis of the consolidation process by the isotaches method. In: Proceedings of the fourth international conference on soil mechanics and foundation engineering, pp 200–206
48. Terzaghi K, Peck RB, Mesri G (1996) Soil mechanics in engineering practice, 3rd edn. Wiley, New York
49. Wang YH, Xu D (2007) Dual porosity and secondary consolidation. J Geotech Geoenviron Eng 133(7):793–801
50. Yin JH, Zhu JG, Graham J (2002) A new elastic viscoplastic model for time-dependent behaviour of normally and overconsolidated clays: theory and verification. Canad Geotech J 39(1):157–173